# Provably Efficient Quantum Algorithms for Solving Nonlinear Differential Equations Using Multiple Bosonic Modes Coupled with Oubits

Yu Gan, <sup>1,\*</sup> Hirad Alipanah, <sup>2,\*</sup> Jinglei Cheng, <sup>1</sup> Zeguan Wu, <sup>1</sup> Guangyi Li, <sup>1,3</sup>

Juan José Mendoza-Arenas, <sup>2,4</sup> Peyman Givi, <sup>2,5</sup> Mujeeb R. Malik, <sup>6</sup> Brian J. McDermott, <sup>7</sup> and Junyu Liu<sup>1,†</sup>

<sup>1</sup> Computer Science, University of Pittsburgh, Pittsburgh, PA 15261, USA

<sup>2</sup> Mechanical Engineering and Materials Science, University of Pittsburgh, Pittsburgh, PA 15261, USA

<sup>3</sup> Electrical Engineering and Computer Science, University of Michigan, Ann Arbor, MI 48109, USA

<sup>4</sup> Physics and Astronomy, University of Pittsburgh, Pittsburgh, PA 15261, USA

<sup>5</sup> Petroleum Engineering, University of Pittsburgh, Pittsburgh, PA 15261, USA

<sup>6</sup> NASA Langley Research Center, Hampton, VA 23681, USA

<sup>7</sup> Naval Nuclear Laboratory, Schenectady, NY 12301, USA

(Dated: November 14, 2025)

**Quantum computers have long been expected to efficiently** solve complex classical differential equations. Most digital, fault-tolerant approaches use Carleman linearization to map nonlinear systems to linear ones and then apply quantum linear-system solvers. However, provable speedups typically require digital truncation and full fault tolerance, rendering such linearization approaches challenging to implement on current hardware. Here we present an analog, continuous-variable algorithm based on coupled bosonic modes with qubit-based adaptive measurements that avoids Hilbert-space digitization. This method encodes classical fields as coherent states and, via Kraus-channel composition derived from the Koopman-von Neumann (KvN) formalism, maps nonlinear evolution to linear dynamics. Unlike many analog schemes, the algorithm is provably efficient: advancing a first-order, L-grid point, d-dimensional, order-K spatialderivative, degree-r polynomial-nonlinearity, strongly dissipative partial differential equations (PDEs) for T time steps costs  $\mathcal{O}(T(\log L + dr \log K))$ . The capability of the scheme is demonstrated by using it to simulate the one-dimensional Burgers' equation and two-dimensional Fisher-KPP equation. The resilience of the method to photon loss is shown under strong-dissipation conditions and an analytic counterterm is derived that systematically cancels the dominant, experimentally calibrated noise. This work establishes a continuous-variable framework for simulating nonlinear systems and identifies a viable pathway toward practical quantum speedup on near-term analog hardware.

#### I. INTRODUCTION

Quantum computing, as suggested by Richard Feynman [1], is naturally suitable for quantum physics—related problems such as chemical systems and many-body dynamics [2]. Quantum algorithms have demonstrated theoretical speedups

over their classical counterparts for problems such as integer factorization [3], unstructured search [4], and linear system solving [5]. Some of the use cases of quantum algorithms are designed not only for quantum systems but also for classical problems [6]. Although significant progress has been made on algorithm development, many of those algorithms require fully fault-tolerant digital architectures that are not yet available.

Numerical simulation of differential equations is of significant interest in many fields, not only in quantum but also in classical systems such as fluid dynamics, to economics, finance, and more [7–41]. In computational fluid dynamics (CFD), the complexity of the flow increases as the Reynolds number Re increases. In classical direct numerical simulation (DNS), the number of grid points needed to resolve all length and time scales increases as  $\mathcal{O}(Re^{9/4})$  [42, 43]. As in quantum many-body physics, simulating turbulence suffers from rapid growth in the effective system size.

Most of the quantum algorithms proposed with rigorous speedup are based on quantum linear system solvers, such as the Harrow–Hassidim–Lloyd (HHL) algorithm [5] and its variants. These solvers typically employ Carleman linearization [44] to embed nonlinear dynamics into a truncated high-dimensional linear system, followed by a quantum linear solver to simulate its evolution [9]. To avoid the "dimensional explosion" in the truncated linear system, there must be a limit on the nonlinearity of the dynamics [9]. These HHL-based quantum algorithms demand fully fault-tolerant digital systems requiring extra overhead in qubit count, circuit depth, and state preparation. Such requirements make linearization-based quantum algorithms impractical for current quantum devices, and the additional challenge of controlling truncation errors further limits their feasibility.

Contemporaneous with Carleman's proposal of linearization for nonlinear systems, Koopman and von Neumann [45, 46] developed an abstract functional-analytic interpretation for nonlinear equations. The method is known as the Koopman–von Neumann (KvN) formalism by which a nonlinear equation can be associated with infinitely many linear equations embedded in an artificial Hilbert space. This

<sup>\*</sup> These authors contributed equally to this work.

<sup>†</sup> junyuliu@pitt.edu

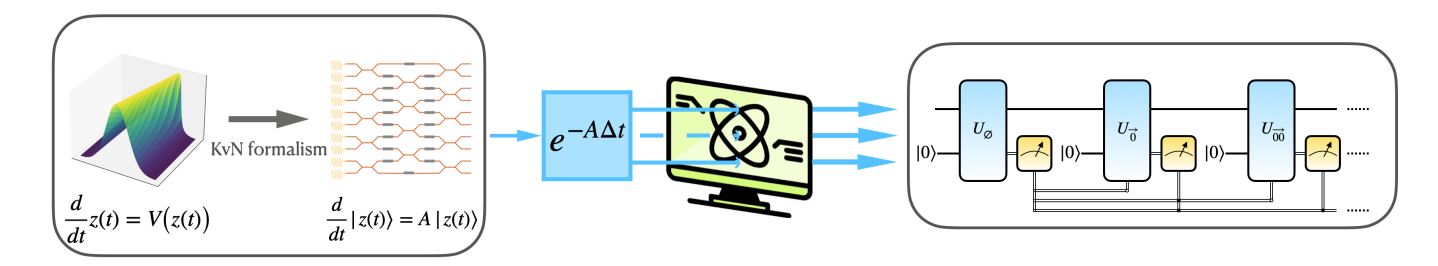


FIG. 1. Overview of the continuous-variable quantum algorithm. Left: A nonlinear field evolution  $\dot{z}=V\left(z(t)\right)$  is lifted by the KvN map to a linear operation generated by A (which encodes the differential equation information) on an enlarged space. Middle: Each short step is implemented as a local CPTP map  $K_a=e^{-A\Delta t}$  acting on bosonic modes prepared in multimode coherent states that encode the classical field. Right:  $K_a$  is compiled into a measurement-adaptive binary-tree circuit: a system-ancilla unitary U, measurement and reset at each layer, and post-selection on  $|0\rangle$  yield logarithmic circuit depth in the Kraus rank.

emergent Hilbert space neither complies with Born's rule nor exhibits entanglement as in quantum physics. Instead, it provides an efficient, quantum-like mathematical description of the original nonlinear dynamics, whether quantum or classical. Thus, Carleman's linearization approaches can be understood as a finite-dimensional digital truncation of this Hilbert space. (This truncation puts a limit on the extent of nonlinearity that can be dealt with by Carleman's linearization). A somewhat similar approach is followed in machine learning through the kernel method and support vector machines, which linearize nonlinear data into a higher-dimensional feature space [47].

In this work, it is shown that the KvN Hilbert space can be generated by multiple bosonic modes, i.e. multiple products of Fock spaces, where the time evolution in differential equations is represented by the dynamics of coherent states. This mapping enables the development of new quantum algorithms in continuous-variable quantum devices. workflow of the algorithm is depicted in Fig. 1, and the procedure goes as follows: the initial condition profiles are uploaded onto coherent states. These states evolve through quantum control following the target differential equations, concluded with the measurement of the annihilation operators to extract the solution. The algorithm also provides a scaling advantage. For highly dissipative equations, time evolution can be treated as dissipative open-system dynamics in multiple bosonic modes. This dynamics is described as a quantum channel or a completely positive trace-preserving (CPTP) map with post-selection for some Kraus rank. Ouantum control theory established in circuit quantum electrodynamics (circuit QED) [48–50] shows that for Kraus rank-N, only  $O(\log N)$  circuit depth is needed to construct the corresponding quantum channel via couplings between bosonic modes and qubits. For ordinary differential equations (ODEs), the Kraus rank is upper-bounded by the number of functions to be solved, and for partial differential equations (PDEs), it is upper-bounded by the number of grid points in spatial discretization. Since large-scale simulations of differential equations such as the Navier-Stokes [6] require of order of billions of grid points, algorithms with logarithmic scaling in circuit depth provide practical benefits. The scaling observed

here is also consistent with the results in Ref. [9]. The tree-like structure of quantum control (Fig. 2) can be understood as a continuous-variable counterpart of conditional rotations in HHL or the tree-like architecture in quantum random access memories (QRAMs) [51].

The bosonic space naturally avoids digital truncation and truncation errors, and significantly reduces the overheads of HHL. Beyond circuit QED, the proposed algorithm may also be implemented in photonics [52], ion traps [53], or neutral atom arrays [54], where bosonic modes with photons can host hundreds of energy levels with strong nonlinearity in emergent Hilbert space. Although fault tolerance remains challenging in analog, bosonic, continuous-variable setups [55], we argue that for strongly dissipative systems and some noise models there exists natural noise resilience. Some quantum noise channels, appearing as additional terms in differential equations (e.g., photon loss), can be suppressed during longtime evolution, making the solutions robust. In addition, an error mitigation technique is developed to reduce the effect of errors by introducing counterterms. Unlike existing proposals, the method developed here can deal with arbitrarily large nonlinearities at a linearly increasing cost. The algorithm also provides some insights into why some of the quantum computing algorithms can efficiently solve highly nonlinear classical problems. These problems suggest the emergence of an artificial Hilbert space from the KvN formalism. Some quantum computing algorithms can mimic this emergent space using the real, physical Hilbert space of quantum mechanics *[56, 57]*.

#### II. KOOPMAN-VON NEUMANN FORMALISM FOR QUANTUM INFORMATION

The Koopman–von Neumann (KvN) formalism trades nonlinearity in the original variables for linear evolution in an enlarged Hilbert space. Recall the properties of a bosonic mode with annihilation operator a (  $[a,a^{\dagger}]=1$ ). One can define the unnormalized coherent state as  $|z\rangle=e^{za^{\dagger}}\,|0\rangle$ . The state satisfies  $a\,|z\rangle=z\,|z\rangle$  and  $a^{\dagger}\,|z\rangle=\frac{\partial}{\partial z}\,|z\rangle$ , which are known as Segal–Bargmann identities. The derivation is pro-

vided in the Supplementary Materials A 1. For the scalar ODE  $\frac{d}{dt}z(t)=V\left(z(t)\right)$ , one can encode the evolution of z into the coherent state variable. Using the chain rule of differentiation, it is straightforward to show that the evolution of the resulting coherent state is  $\frac{d}{dt}|z(t)\rangle=a^{\dagger}|z(t)\rangle\cdot V(z(t)).$  Applying the Segal–Bargmann identities, the operator V can be re-written such that  $V(a)\,|z\rangle:=V(z)\,|z\rangle$ . Defining an effective operator  $A:=a^{\dagger}V(a)$ , the original nonlinear ODE is mapped into the linear evolution:

$$\frac{d}{dt}|z(t)\rangle = A|z(t)\rangle. \tag{1}$$

The trajectory z(t) can be recovered using

$$z(t) = \frac{\langle z(t) | a | z(t) \rangle}{\langle z(t) | z(t) \rangle}, \tag{2}$$

which follows directly from the Segal-Bargmann identities. In the model developed here, the nonlinear flow in z is encoded into the amplitudes of the coherent state  $|z\rangle$  and the nonlinear evolution of z is mapped to a linear evolution for  $|z\rangle$ . The method can be generalized to the multivariate case. Let  $z(t) = (z_1(t), \dots, z_n(t))$ . The corresponding multimode coherent state is the tensor product  $|z(t)\rangle = \bigotimes_i |z_i(t)\rangle$ , and each  $z_i(t)$  is governed by a corresponding nonlinear ODE. The general coherent state is now defined as the tensor product of the coherent states corresponding to each  $z_i(t)$ . It is easy to verify that the bosonic mode property and the Segal-Bargmann identities can be extended to the multivariate case, which can be constructed with the transformed state  $|z(t)\rangle$ . As in the univariate case, an effective operator A(t) is defined for the original vector field operator. Expanding the original vector field operator corresponding to  $z_i(t)$  in monomials with coefficients  $c_{j,k_1...k_m}(t)$  gives the normal-order generator:

$$A(t) = \sum_{j=1}^{n} a_{j}^{\dagger} \left( \sum_{m=0}^{\infty} \sum_{k_{1},\dots,k_{m}=1}^{n} c_{j,k_{1}\dots k_{m}}(t) \ a_{k_{1}} \cdots a_{k_{m}} \right).$$
(3)

For a polynomial vector field with nonlinearity of degree r, the inner sum truncates at  $m \leq r$ . With the KvN formalism, the transformed state  $|z(t)\rangle$  evolves linearly under the operator A(t). Moreover, by projecting the transformed state back using Eq. (2), the original dynamics is recovered. A detailed description is provided in the Supplementary Materials A 2.

There exists a transparent link between our method and Carleman linearization. When the differential operator at the grid point j, denoted by  $F_j$ , has a polynomial nonlinearity of degree r, we see that  $F_j(a)$  contains r annihilators and  $a_j^{\dagger}$  increases the degree by one. Consequently, A couples number-state sectors of total degree m only to degrees up to m+(r-1). This is the same "degree bandwidth" that appears when stacking monomials  $(z,z^{\otimes 2},z^{\otimes 3},\dots)$  in Carleman's construction to obtain a linear ODE [58]. Projecting the KvN evolution so that it includes only polynomial terms up to degree K gives the same result as a degree-K Carleman truncation, while the degree-1 block read out via Eq. (2)

reproduces the solution to the original dynamics. In the next sections, we will introduce how to use the Kraus representation and quantum channel to solve the PDE with the KvN formulation. In the Supplementary Materials D, we discuss the alternative way to solve PDE in KvN formulation using Trotterization method and show that it leads to the same forward Euler equation.

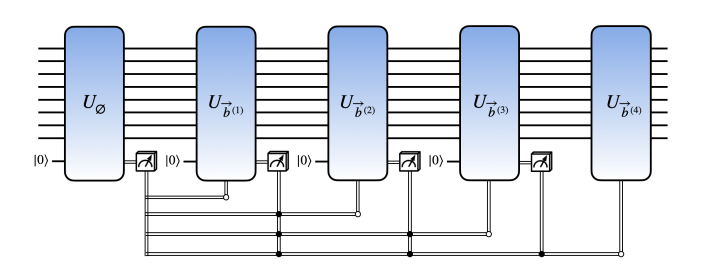
#### III. KRAUS REPRESENTATION

According to Choi's theorem, any completely positive trace-preserving (CPTP) map from Hilbert space  $\mathcal{H}_A$  to Hilbert space  $\mathcal{H}_B$ ,  $\mathcal{N}:\mathcal{L}(\mathcal{H}_A)\to\mathcal{L}(\mathcal{H}_B)$ , admits a Kraus decomposition  $\mathcal{N}(X)=\sum_{b\in\mathcal{B}}K_b\,X\,K_b^\dagger,\ \forall X\in\mathcal{L}(\mathcal{H}_A)$  with Kraus operators satisfying  $\sum_{b\in\mathcal{B}}K_b^\dagger K_b=\mathbb{I}$ . To implement Kraus operators, we couple the bosonic register with a single ancilla qubit initialized in  $|0\rangle$ . Then, we apply a joint unitary to the coupled system and perform a projective measurement on the ancilla qubit. When the outcome is  $b\in\mathcal{B}$ , the system undergoes the evolution governed by  $K_b$ . We designate a post-selected "successful" branch  $a\in\mathcal{B}$  (outcome  $|0\rangle$ ), parametrized as

$$K_a = e^{-A \Delta t}, \quad \sum_{b \neq a} K_b^{\dagger} K_b = \mathbb{I} - K_a^{\dagger} K_a,$$
 (4)

with  $A \succeq 0$  a positive semidefinite generator. In the simplest nontrivial case  $|\mathcal{B}| = 2$ , this reduces to  $K_a = e^{-A\Delta t}$  and  $K_{\bar{a}} = \sqrt{\mathbb{I} - K_a^{\dagger} K_a}$ . For general rank-N channels  $(|\mathcal{B}| = N)$ , the other branches  $\{K_b\}_{b \neq a}$  are supplied recursively by QR/SVD completion inside a binary-tree structure.

To compile this Kraus-decomposition-based postselectioninvolved dynamics into a shallow circuit, we adopt the binarytree construction from [48, 49]. A CPTP map of Kraus rank N is decomposed into  $\lceil \log_2 N \rceil$  adaptive rounds of ancilla interaction, measurement, and feed-forward. In round l, a joint system–ancilla unitary  $U_{\mathbf{b}^{(\ell-1)}}$  is applied, where  $\mathbf{b}^{(\ell-1)}=(b_1,\dots,b_{\ell-1})$  records the results of all previous ancilla measurements. The tree therefore branches adaptively: the root corresponds to  $U_{\varnothing}$ , the next layer selects  $U_0$  or  $U_1$ depending on  $b_1$ , and so on. This architecture, illustrated in the left side of Fig. 2, realizes depth  $\mathcal{O}(\log N)$ , in contrast to a textbook Stinespring dilation which in general requires an environment of dimension  $d^2$  (corresponding to  $N=d^2$ ) and a joint unitary in  $SU(d^3)$  for a d-dimensional system [59]. In our setting, we do not compile the full channel but instead focus on a single post-selected trajectory: only branches with  $b_{\ell} = 0$  are retained (post-selection on  $|0\rangle$ ), directly enforcing the target Kraus operator  $K_a$ . This selective evolution is particularly natural in circuit-QED platforms, where ancilla reset and high-fidelity measurement are available in each round. A concrete demonstration is given on the right side of Fig. 2. This explicit construction verifies that the binary-tree procedure yields a complete set of channels satisfying the Kraus consistency condition.



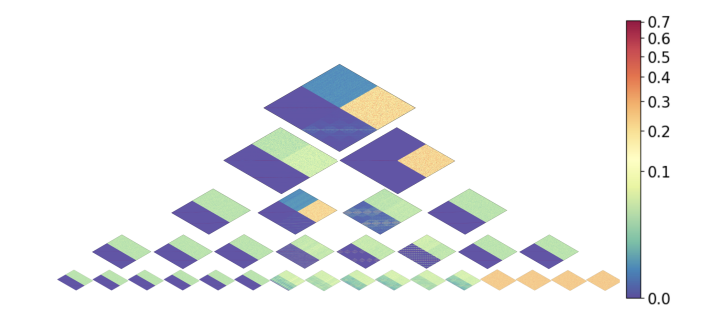


FIG. 2. Circuit realization and unitary construction for a 1D Burgers' equation. Left: Measurement-adaptive binary-tree realization of an N-rank-Kraus-operator CPTP map using a single ancilla qubit [49]. At depth  $\ell$ , the joint unitary  $U_{\mathbf{b}(\ell-1)}$  is applied, where  $\mathbf{b}^{(\ell-1)}$  records the past measurement outcomes. After each interaction, the ancilla is measured and reset. Post-selection on  $|0\rangle$  (empty-circle control) singles out the Kraus operator  $K_a$ . Right: Magnitude plots of all compiled block unitaries  $U_{\mathbf{b}}$  for a four-mode bosonic system truncated to four levels per mode ( $d_{\mathrm{sys}} = 256$ ), arranged hierarchically from the root ( $U_{\varnothing}$ ) to depth-4 leaves ( $U_{0000}, \ldots, U_{1111}$  with subscripts in the lexicographical order). For each  $U_{\mathbf{b}}$ , the left half encodes the analytically derived Kraus block  $\langle b_{\ell+1}|U_{\mathbf{b}}|0\rangle$ , while the right half shows the QR-completed orthonormal complement required to form a valid unitary.

## IV. QUANTUM CHANNEL EXECUTION AND SAMPLING OVERHEAD

We implement the short-time Kraus channel using measurement-conditioned unitaries and separate the spatial and temporal contributions to the cost. At each step  $\Delta t$ , the system–ancilla interaction realizes an N-outcome map  $\rho\mapsto\sum_{b\in\mathcal{B}}K_b\rho K_b^\dagger$  with the short-time parameterization of Eq. (4), where  $\rho$  denotes the system's density operator, representing its quantum state. Post-selection on a designated outcome  $a\in\mathcal{B}$  (ancilla state  $|0\rangle$ ) enforces  $K_a$  with success probability

$$p_a = \operatorname{Tr}\left(K_a^{\dagger}K_a\rho\right) \approx 1 - 2\Delta t \cdot \operatorname{Tr}\left(A\rho\right) + \mathcal{O}(\Delta t^2).$$
 (5)

To ensure that the outcome of the ancillary measurement corresponds to  $K_a$  with probability  $p_a$  greater than  $1 - \epsilon$ , it suffices to choose a time step  $\Delta t$  that satisfies the following:

$$\Delta t \leq \frac{\epsilon}{2 \operatorname{Tr} (A\rho)}.$$
 (6)

The value  ${\rm Tr}(A\rho)$  depends on the system state  $\rho$ , which includes a factor z. Specifically, z is defined as the solution of the eigenvalue equation  $a\,|z\rangle\,=\,z\,|z\rangle$ , where a is the annihilation operator. In strongly dissipative regimes, z typically decays exponentially over time [60], so  ${\rm Tr}(A\rho)$  becomes very small at late times. This implies that the step size constraint on  $\Delta t$  becomes increasingly relaxed as the system evolves, especially in the long-time limit. A detailed analysis of  ${\rm Tr}(A\rho)$  is provided in the Supplementary Materials B 1.

**Spatial vs. Temporal cost:** We treat space and time separately: (i) the *spatial* cost is the circuit depth per step to realize the post-selected branch; (ii) the *temporal* cost is the number of steps needed to reach a physical time T under the step-size restriction above. Throughout this section, d denotes the spatial dimension, L the number of grid points,  $\mathcal{N}_R(i)$  the Manhattan neighborhood of radius R at grid point i, K the highest spatial-derivative order encoded by the stencil (typically

 $R = \Theta(K)$ , as proved in the Supplementary Materials B 2), and r the degree of nonlinearity in normal-ordered monomials.

**Theorem IV.1** (Kraus Rank and Circuit Depth for Linear Generators). *Consider the linear PDEs of L grid points:* 

$$\frac{\partial u_i}{\partial t} = \sum_{j \in \mathcal{N}_R(i)} c_{ij} \, u_j, \qquad i = 1, \dots, L. \tag{7}$$

The generator corresponding to this system is a linear and positive operator of the form  $A = \sum_{(i,j) \in E} \alpha_{ij} \, a_i^{\dagger} a_j$ , where  $E = \{(i,j) : j \in \mathcal{N}_R(i)\}$  is a bounded-degree directed stencil and the coefficients  $\alpha_{ij}$  are chosen to have the same sparsity as  $c_{ij}$ . A short-time CPTP realization exists that assigns two non-identity Kraus operators to each directed coupling  $(i,j) \in E$ . The Kraus rank is therefore N = 2|E|. For a nearest-neighbor lattice where  $|E| = \mathcal{O}(dL)$ , the rank becomes  $N = \mathcal{O}(dL)$ . The per-step circuit depth for a binary-tree implementation of this channel scales as  $\mathcal{O}(\log N) = \mathcal{O}(\log(dL))$ , up to additive constants depending on the dimension d.

Based on Theorem IV.1, we now consider nonlinear partial differential equations whose nonlinearities are polynomial:

$$\frac{\partial u_i}{\partial t} = \sum_{\alpha} c_{i,\alpha} \prod_{m=1}^r u_{j_m^{(\alpha)}}, \ j_m^{(\alpha)} \in \mathcal{N}_R(i), \ i = 1, \dots, L.$$
(8)

The associated *polynomial* generator uses the same normal-ordered monomials and support, is defined as  $A=\sum_{i,\alpha}L_{i,\alpha}$  with  $L_{i,\alpha}=a_i^\dagger\prod_{m=1}^ra_{j_m^{(\alpha)}}$ . Here r is the degree of nonlinearity and the factors  $a_{j_m^{(\alpha)}}$  act within the neighborhood  $\mathcal{N}_R(i)$ .

**Theorem IV.2** (Kraus Rank and Circuit Depth for Polynomial Generators). On a d-dimensional lattice with L grid points, nonlinearity degree r, and stencil order K, the total Kraus rank is  $\mathcal{O}(L K^{dr})$  and the depth of the binary-tree per-step is  $\mathcal{O}(\log N) = \mathcal{O}(\log L + dr \log K)$ .

The proofs of Theorems IV.1–IV.2 are provided in the Supplementary Materials B.

From Eq. (6), the number of successful steps to reach T is at least  $\Theta \left( T\operatorname{Tr}(A\rho)/\epsilon \right)$ . For fixed K, r, each physical step costs  $\mathcal{O}(\log L + dr\log K)$  depth, while the step count is controlled by  $\operatorname{Tr}(A\rho)$ . The total cost to reach time T is therefore upperbounded by

$$\underbrace{\mathcal{O}(\log L + dr \log K)}_{\text{depth per step}} \times \underbrace{\Theta \big( T \operatorname{Tr}(A\rho)/\epsilon \big)}_{\text{accepted steps}}.$$

In practice, the actual Kraus rank, and the total cost can be much less than the given bounds.

#### V. NUMERICAL SIMULATION

We simulate our continuous-variable quantum algorithm in a coherent-state framework. Rather than evolving the full density operator, we propagate observables by tracking coherent amplitudes and their variances. In this section, we focus on 1D Burgers' equation and 2D Fisher-KPP dynamics. At each grid point we assume a Gaussian readout model whose mean equals to the deterministic PDE solution and whose variance is predicted by the first-order moment formulas derived in Supplementary Materials C1 and C3. At each saved time we sample  $N=10^4$  i.i.d. shots per grid point, compute the sample mean and the unbiased sample variance  $Var_{\rm em}$ , and compare them with the theoretical predictions u and  $Var_{th}$ ; the expected relative  $1\sigma$  fluctuation of  $Var_{em}$  is  $\sqrt{2/(N-1)}$ . Fig. 3 and Fig. 4 present the corresponding mean field and the sample-mean residual, while Table I and Table II compare Var<sub>em</sub> and Var<sub>th</sub>.

In the Supplementary Materials we also describe a Trotterization-based algorithm for the lid-driven cavity Navier–Stokes flow and provide the tensor network simulation of the Burgers' equation for demonstrating the Trotterization algorithm's feasibility.

#### A. 1D Burgers' Equation

The viscous Burgers' equation is a canonical nonlinear advection—diffusion model and a standard testbed for transport with viscosity:

$$\frac{\partial u}{\partial t} = -u \frac{\partial u}{\partial x} + \frac{1}{R_e} \frac{\partial^2 u}{\partial x^2}.$$
 (9)

In the coherent-state simulation, we propagate a single deterministic mean-field solution u(x,t) using the Forward-Euler update rule in Eq. (C33), and adopt a Gaussian readout model with variance given by the first-order moment formula in Eq. (C36) at each grid point. For each saved time between 0 and 0.24 s we draw  $N=10^4$  i.i.d. shots per grid point, compute the sample mean and the unbiased sample variance  $Var_{\rm em}$ , and compare them with the theoretical predictions u

t(s)	$\overline{\mathrm{Var}}_{\mathrm{th}}$	$\overline{\mathrm{Var}}_{\mathrm{em}}$	relBias	$\operatorname{rel} L^2$
0.00	3.534144	3.532065	$-5.883 \times 10^{-4}$	$1.398 \times 10^{-2}$
0.06	3.534144	3.533156	$-2.795 \times 10^{-4}$	$1.523 \times 10^{-2}$
0.12	3.534144	3.532177	$-5.567 \times 10^{-4}$	$1.529 \times 10^{-2}$
0.18	3.534144	3.530277	$-1.094 \times 10^{-3}$	$1.546 \times 10^{-2}$
0.24	3.534144	3.525037	$-2.577 \times 10^{-3}$	$1.380 \times 10^{-2}$

TABLE I. Burgers variance (empirical vs. theoretical). All reported variances are of order  $10^{-5}$  or smaller, underscoring that noise around the mean-field trajectory remains extremely weak. We report  $\overline{\text{Var}_{\text{th}}}$ ,  $\overline{\text{Var}_{\text{em}}}$ , the relative bias relBias =  $(\overline{\text{Var}_{\text{em}}} - \overline{\text{Var}_{\text{th}}})/\overline{\text{Var}_{\text{th}}}$ , and the per-time global relative  $L^2$  error rel  $L^2$  =  $\|\text{Var}_{\text{em}} - \text{Var}_{\text{th}}\|_2/\|\text{Var}_{\text{th}}\|_2$ ; an overbar denotes an average over grid points. For  $N=10^4$ , the theoretical sampling envelope is  $\sqrt{2/(N-1)}=1.414\times10^{-2}$ , which lies within the per-time relative  $L^2$  values reported in the table and is consistent with finite-N sampling noise.

and  $Var_{\rm th}$ . The expected relative  $1\sigma$  fluctuation of  $Var_{\rm em}$  is  $\sqrt{2/(N-1)}\approx 1.414\times 10^{-2}$ . Table I reports the spatially averaged theoretical and empirical variances, while Fig. 3 shows the mean fields and the sample-mean residuals. The samplemean residuals are zero-mean with a speckle-like appearance and nearly time-invariant contrast, consistent with a leading-order time-independent readout variance  $Var_{\rm th}$  [Eq. (C36)]. A tensor network simulation of the Burgers' equation for demonstrating the Trotterization algorithm's feasibility is also provided in the Supplementary Materials E.

#### B. 2D Fisher-KPP Dynamics

We next consider the 2D Fisher–KPP equation as a canonical reaction–advection–diffusion benchmark to illustrate our continuous-variable framework on a rotating flow. The 2D Fisher-KPP equation involves the diffusion and reaction of a scalar variable advected by a known velocity field.

$$\frac{\partial u}{\partial t} + v_x \frac{\partial u}{\partial x} + v_y \frac{\partial u}{\partial y} = \frac{1}{\text{Pe}} \left( \frac{\partial^2 u}{\partial x^2} + \frac{\partial^2 u}{\partial y^2} \right) + \text{Da} \left[ u(1-u) \right].$$

The derivations of the mean and variance of the corresponding z are provided in the Supplementary Materials C 3 a. We quantitatively compare the theoretical variance  ${\rm Var}_{\rm th}$  from Eq. (C54) with the empirical variance  ${\rm Var}_{\rm em}$  obtained from  $N=10^4$  shots per grid point in Table II (theoretical relative  $1\sigma$  for the sample variance is  $\sqrt{2/(N-1)}\approx 1.414\times 10^{-2}$ ). Spatial means and global relative bias are reported in Fig. 4; results agree with theory within sampling fluctuations across the evolving vortex structures. This result confirms that Eqs. (C51)–(C54) correctly capture rotational transport, diffusion, and nonlinear growth to first order in  $\Delta t$ .

#### VI. NOISE RESILIENCE

The influence of environmental noise on the bosonic quantum simulation is captured by open-system dynamics. The

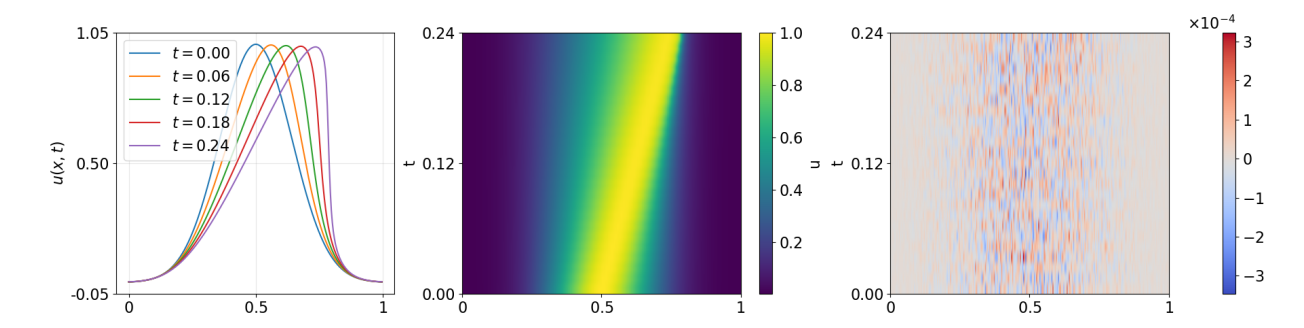


FIG. 3. **1D Burgers' validation.** Left: mean-field solution profiles at selected times. The results demonstrate the rightward advection with speed set by u, nonlinear steepening from the advective term  $-u\partial u/\partial x$  together with diffusive broadening from  $1/R_e \cdot \partial^2 u/\partial x^2$ . Middle: spacetime map of the mean field u(x,t) over the entire evolution window, showing advection-dominated rightward drift with weak viscous spreading. Right: Sample-mean bias using  $N=10^4$  shots per grid point. The residuals are centered around zero and spatially unstructured, consistent with the prediction that  $\mathrm{Var}_j(t)$  remains constant and time-independent to first order [Eq. (C43)], so that sampling fluctuations are the only visible deviations.

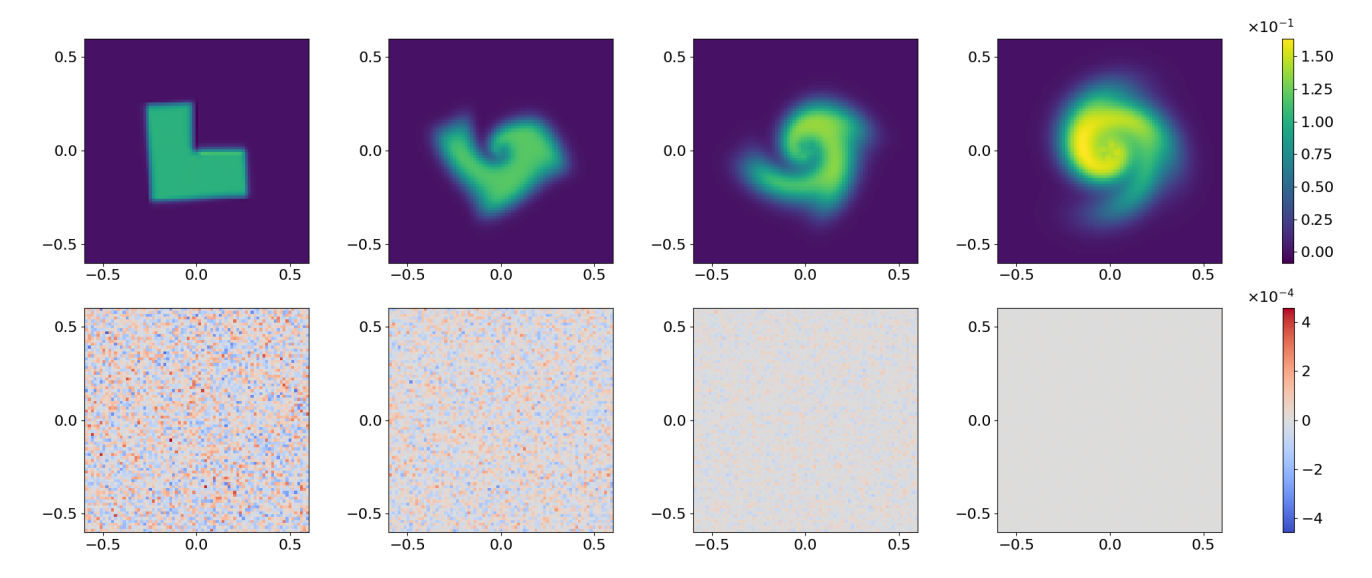


FIG. 4. **2D Fisher-KPP validation.** Row 1: analytic mean fields u(x,y,t) at representative times  $t=0.02,\ 0.20,\ 0.40,\ 0.80$  s, showing the rotational advection imposed by the velocity field, the smoothing action of diffusion (Pe = 200), and the amplitude saturation from the Fisher reaction term (Da = 1). Row 2: Bias maps from  $N=10^4$  trajectories. The residuals remain centered around zero with no coherent structure, confirming that the stochastic sampling is unbiased. The omitted panels for the predicted  $1\sigma$  noise width and the empirical-to-analytic error-bar ratio behave as in Supplementary Materials C 3 a, i.e. Gaussian fluctuations with variance  $V_{p,q}(t)$  that scale as  $\sigma/\sqrt{N}$ . Together, the results validate the analytic update formulas (C51)–(C54) across the evolving vortex and front structures.

evolution of the density matrix  $\rho$  of the mixed bosonic state is governed by a Lindblad master equation that incorporates both the coherent generator M and the dominant noise channel. Photon loss is considered as the primary decoherence mechanism in typical bosonic platforms [61–63]. The master equation is written as:

$$\frac{\partial \rho}{\partial t} = M\rho + \rho M^{\dagger} + \sum_{j=1}^{n} \left[ \gamma a_{j} \rho a_{j}^{\dagger} - \frac{\gamma}{2} \{ a_{j}^{\dagger} a_{j}, \rho \} \right], \quad (10)$$

where  $\gamma$  denotes the photon loss rate. The dissipator corresponds to amplitude damping. For analytical tractability, the state is expressed in the diagonal coherent-state representation

via

$$\rho(t) = \int P(z, z^*, t) |z\rangle \langle z| d^2 z, \qquad (11)$$

with  $d^2z=\prod_{j=1}^n d^2z_j$  and  $P(z,z^*,t)$  being a quasi-probability distribution (the generalized Glauber-Sudarshan P-function) [64]. Substitution of this ansatz into the master equation leads to a partial differential equation for P, which, after standard manipulations, takes the form of a generalized Fokker–Planck equation (F9). Under the assumption that non-linearities in  $F_j$  are sufficiently smooth and that P remains well approximated by a Gaussian-like peak in phase space, the evolution of the first moments (the coherent amplitudes) is extracted. The drift terms emerging from this analysis yield the following effective evolution for the coherent amplitudes:

t (s)	$\overline{\mathrm{Var}}_{\mathrm{th}}$	$\overline{\mathrm{Var}}_{\mathrm{em}}^{\mathrm{mean}}$	relBias	$\operatorname{rel} L^2$
0.02	14.067745	14.067418	$-2.326 \times 10^{-5}$	$+1.414\times10^{-2}$
0.20	6.326569	6.325933	$-1.005 \times 10^{-4}$	$+1.407\times10^{-2}$
0.40	0.997785	0.997726	$-5.907 \times 10^{-5}$	$+1.410\times10^{-2}$
0.80	0.001421	0.001421	$+2.130\times10^{-4}$	$+1.402\times10^{-2}$

TABLE II. Fisher-KPP variance (empirical vs. theoretical). Reported variances are  $\mathcal{O}(10^{-5})$ , consistent with extremely weak noise. We report  $\overline{\mathrm{Var}}_{\mathrm{th}}$ ,  $\overline{\mathrm{Var}}_{\mathrm{em}}$ , the relative bias relBias =  $(\overline{\mathrm{Var}}_{\mathrm{em}} - \overline{\mathrm{Var}}_{\mathrm{th}})/\overline{\mathrm{Var}}_{\mathrm{th}}$ , and the per-time global relative  $L^2$  error rel  $L^2 = \|\mathrm{Var}_{\mathrm{em}} - \mathrm{Var}_{\mathrm{th}}\|_2/\|\mathrm{Var}_{\mathrm{th}}\|_2$ ; the bar denotes averaging over grid points. For  $N = 10^4$ , the theoretical sampling envelope is  $\sqrt{2/(N-1)} = 1.414 \times 10^{-2}$ , which lies within the per-time relative  $L^2$  values reported here.

$$\frac{dz_k}{dt} = F_k(z) - \frac{\gamma}{2} z_k \tag{12}$$

where the  $-\frac{\gamma}{2}z_k$  term represents exponential decay due to photon loss. The details of this derivation are provided in the Supplementary Materials F. The dominant degradation is therefore a multiplicative decay of amplitude with rate  $\gamma/2$ . When higher-order dissipative effects become non-negligible, corrections proportional to  $\gamma^2$  or nonlinear couplings between loss and the dynamics can be derived by retaining higher cumulants in the expansion of P. In parallel, stochastic unravelings such as the quantum-trajectory (Monte Carlo wavefunction) method provide an approximation of the Lindblad dynamics for any  $\gamma$ . Therefore, they can be used to benchmark and quantify deviations from the truncated Gaussian-peak approximation [64, 65].

The solution of Eq. (12) is

$$z_k(t) = \tilde{z}_k(t) \exp\left(-\frac{\gamma}{2}t\right),$$
 (13)

where  $\tilde{z}_k(t)$  denotes the ideal noiseless evolution satisfying  $\frac{d\tilde{z}_k}{dt} = F_k(\tilde{z})$ . Consequently, the measured expectation values are attenuated relative to their ideal counterparts, and this systematic decay can be compensated for if the loss rate is estimated. Therefore, a time-local correction (counterterm) is implemented by multiplying the solution profile by an exponential term  $\exp{(\bar{\gamma}t/2)}$  where  $\bar{\gamma}$  is the estimate of  $\gamma$ . This term effectively inverts exponential damping. The estimated loss rate  $\bar{\gamma}$  can be characterized experimentally through coherent state decay measurements and performed on a calibration schedule to infer the effective Lindblad parameters.

Residual errors arising from imperfect knowledge of  $\gamma$ , higher-order cross terms, or non-Gaussian distortions can be further suppressed by combining the analytic correction with extrapolation techniques. For example, a sequence of short-time evolutions with varying effective loss rates (achieved by artificially inserting calibrated attenuation) can be used to perform Richardson extrapolation back to the zero-loss limit [66, 67]. In addition, measurement-based feedback can be

used: after each time step, the coherent-state amplitude is estimated, the discrepancy from the expected corrected value is evaluated, and a small coherent displacement is applied to the recenter state, effectively performing a form of state stabilization [68].

The validity of the Gaussian ansatz and linear correction is guaranteed when the loss rate remains small compared to the inverse time step  $(\Delta t)$  and when the nonlinear vector field F(z) does not drive the system into regions of phase space where higher moments become dominant. In stiff or strongly nonlinear regimes, adaptive step-sizing or higher-order noise-aware integrators can be used, with noise-modified commutator expansions in the Trotterization algorithm guiding the required modifications (introduced in Supplementary Materials D).

#### VII. CONCLUSION

We have introduced a provably efficient, continuous-variable quantum algorithm for solving nonlinear PDEs. The key innovation of our work is the application of the KvN formalism to lift nonlinear dynamics into a linear, albeit dissipative, evolution within an infinite-dimensional bosonic Hilbert space.

This method allows for the encoding of classical fields into coherent states of bosonic modes. The dynamics is then implemented as a CPTP map, which we compile into a quantum circuit with a logarithmic depth per time step. Specifically, for a d-dimensional system with L lattice grid points, a polynomial nonlinearity of degree r, and spatial derivatives of order K, the per-step circuit depth scales as  $O(\log L + dr \log K)$ .

This continuous-variable framework provides a significant advantage by sidestepping the truncation errors and substantial resource overhead associated with Carleman linearization-based digital methods. Our high-fidelity numerical simulations of Fisher-KPP equations and the lid-driven cavity problem serve as a robust validation of the algorithm's accuracy and near-term feasibility. Furthermore, we argue that certain forms of noise resilience will occur for highly dissipative quantum systems. The KvN formalism, traditionally a theoretical tool for unifying classical and quantum mechanics, is shown here to be a powerful computational framework, analogous to a kernel method for dynamical systems. By physically realizing the enlarged linear space of the KvN formalism, our approach offers a direct and efficient means of simulating complex nonlinear phenomena. This work establishes a compelling alternative to fault-tolerant digital quantum computing, paving a viable path toward achieving a potential quantum speedup in scientific computing on near-term analog hardware. Future research will be directed towards the experimental implementation of this algorithm and the creation of higher-order, more noise-resilient integrators.

We note that the famous connection between the KvN approach and Carleman linearization has been widely noted in the quantum algorithm community [69-75]. Compared to those works, our primary contribution is to connect KvN with quantum channel and Kraus operator frameworks in quantum information science, and to provide solid arguments about the scaling statement in quantum algorithms. From the digital computing point of view, our algorithm takes a significant leap from high fault-tolerant overhead towards more near-term-feasible routines. A related line of research is the Schrödingerisation method [16, 20, 21, 31], which maps linear or nonlinear PDEs to a Schrödinger-type equation solvable by Hamiltonian simulation after spatial discretization. Although based on the digital truncation approach instead of continuous-variable quantum computing, their approach can, in principle, be combined with the KvN formalism we have developed and runnable on analog quantum hardware.

Acknowledgments—We thank Ken Brown, Andrew Childs, Fred Chong, Jens Eisert, Steve Girvin, Hsin-Yuan Huang, Travis Humble, Liang Jiang, Jin-Peng Liu, and John Preskill for helpful discussions. The authors acknowledge support from the U.S. Air Force Office of Scientific Research (AFOSR) under Grant No. FA9550-23-1-0014. YG, JL, JC, ZW and GL are supported in part by the University of Pittsburgh School of Computing and Information, Department of Computer Science, Pitt Cyber, POI Community Collaboration Awards, John C. Mascaro Faculty Scholar in Sustainability, NASA under award number 80NSSC25M7057, and Fluor Marine Propulsion LLC (U.S. Naval Nuclear Laboratory) under award number 140449-R08. This work has been co-authored by a contractor of the U.S. Government under contract number DOE89233018CNR000004. Accordingly, the U.S. Government retains a non-exclusive, royalty-free license to publish or reproduce the published form of this contribution, or allow others to do so, for U.S. Government purposes.

- [1] R. P. Feynman, Simulating physics with computers, in *Feynman and computation* (CRC Press, 2018) pp. 133–153.
- [2] S. Lloyd, Universal quantum simulators, Science 273, 1073 (1996).
- [3] P. W. Shor, Polynomial-time algorithms for prime factorization and discrete logarithms on a quantum computer, SIAM Journal on Computing **26**, 1484 (1997).
- [4] L. K. Grover, A fast quantum mechanical algorithm for database search, in *Proceedings of the twenty-eighth annual* ACM symposium on Theory of computing (1996) pp. 212–219.
- [5] A. W. Harrow, A. Hassidim, and S. Lloyd, Quantum algorithm for linear systems of equations, Physical review letters 103, 150502 (2009).
- [6] P. Givi, A. J. Daley, D. Mavriplis, and M. Malik, Quantum speedup for aeroscience and engineering, AIAA Journal 58, 3715 (2020).
- [7] S. K. Leyton and T. J. Osborne, A quantum algorithm to solve nonlinear differential equations (2008), arXiv:0812.4423.
- [8] D. W. Berry, High-order quantum algorithm for solving linear differential equations, Journal of Physics A: Mathematical and Theoretical 47, 105301 (2014).
- [9] J.-P. Liu, H. Ø. Kolden, H. K. Krovi, N. F. Loureiro, K. Trivisa, and A. M. Childs, Efficient quantum algorithm for dissipative nonlinear differential equations, Proceedings of the National Academy of Sciences 118, 10.1073/pnas.2026805118 (2021).
- [10] B. T. Kiani, G. De Palma, D. Englund, W. Kaminsky, M. Marvian, and S. Lloyd, Quantum advantage for differential equation analysis, Physical Review A 105, 022415 (2022).
- [11] A. M. Childs and J.-P. Liu, Quantum spectral methods for differential equations, Communications in Mathematical Physics 375, 1427 (2020).
- [12] T. Xin, S. Wei, J. Cui, J. Xiao, I. Arrazola, L. Lamata, X. Kong, D. Lu, E. Solano, and G. Long, Quantum algorithm for solving linear differential equations: Theory and experiment, Physical Review A 101, 032307 (2020).
- [13] A. M. Childs, J.-P. Liu, and A. Ostrander, High-precision quantum algorithms for partial differential equations, Quantum 5, 574 (2021).
- [14] O. Kyriienko, A. E. Paine, and V. E. Elfving, Solving nonlin-

- ear differential equations with differentiable quantum circuits, Phys. Rev. A **103**, 052416 (2021).
- [15] D. An, J.-P. Liu, D. Wang, and Q. Zhao, A theory of quantum differential equation solvers: limitations and fast-forwarding, arXiv preprint arXiv:2211.05246 (2022).
- [16] S. Jin, N. Liu, and Y. Yu, Quantum simulation of partial differential equations: Applications and detailed analysis, Phys. Rev. A 108, 032603 (2023).
- [17] J.-P. Liu, D. An, D. Fang, J. Wang, G. H. Low, and S. Jordan, Efficient quantum algorithm for nonlinear reaction–diffusion equations and energy estimation, Communications in Mathematical Physics 404, 963 (2023).
- [18] Z. Meng and Y. Yang, Quantum computing of fluid dynamics using the hydrodynamic Schrödinger equation, Phys. Rev. Research 5, 033182 (2023).
- [19] Z.-Y. Chen, T.-Y. Ma, C.-C. Ye, L. Xu, W. Bai, L. Zhou, M.-Y. Tan, X.-N. Zhuang, X.-F. Xu, Y.-J. Wang, et al., Enabling large-scale and high-precision fluid simulations on near-term quantum computers, Comput. Methods Appl. Mech. Eng. 432, 117428 (2024).
- [20] S. Jin, N. Liu, and Y. Yu, Quantum simulation of partial differential equations via schrödingerization, Physical Review Letters 133, 230602 (2024).
- [21] S. Jin, X. Li, N. Liu, and Y. Yu, Quantum simulation for partial differential equations with physical boundary or interface conditions, Journal of Computational Physics 498, 112707 (2024).
- [22] J. Liu, M. Liu, J.-P. Liu, Z. Ye, Y. Wang, Y. Alexeev, J. Eisert, and L. Jiang, Towards provably efficient quantum algorithms for large-scale machine-learning models, Nature Communications 15, 434 (2024).
- [23] Z. Lu and Y. Yang, Quantum computing of reacting flows via Hamiltonian simulation, Proc. Combust. Inst. 40, 105440 (2024).
- [24] Z. Meng and Y. Yang, Quantum spin representation for the Navier–Stokes equation, Phys. Rev. Research 6, 043130 (2024).
- [25] Z. Meng, J. Zhong, S. Xu, K. Wang, J. Chen, F. Jin, X. Zhu, Y. Gao, Y. Wu, C. Zhang, *et al.*, Simulating unsteady flows on a superconducting quantum processor, Commun. Phys. 7, 349 (2024).

- [26] H. Su, S. Xiong, and Y. Yang, Quantum state preparation for a velocity field based on the spherical Clebsch wave function (2024), arXiv:2406.04652.
- [27] C.-C. Ye, N.-B. An, T.-Y. Ma, M.-H. Dou, W. Bai, D.-J. Sun, Z.-Y. Chen, and G.-P. Guo, A hybrid quantum-classical framework for computational fluid dynamics, Phys. Fluids 36 (2024).
- [28] H. Alipanah, F. Zhang, Y. Yao, R. Thompson, N. Nguyen, J. Liu, P. Givi, B. J. McDermott, and J. J. Mendoza-Arenas, Quantum dynamics simulation of the advection-diffusion equation, arXiv preprint arXiv:2503.13729 (2025).
- [29] P. C. Costa, P. Schleich, M. E. Morales, and D. W. Berry, Further improving quantum algorithms for nonlinear differential equations via higher-order methods and rescaling, npj Quantum Information 11, 141 (2025).
- [30] D. Fang, D. L. George, and Y. Tong, Qubit-efficient quantum algorithm for linear differential equations, arXiv preprint arXiv:2507.16995 (2025).
- [31] F. Golse, S. Jin, and N. Liu, Quantum algorithms for uncertainty quantification: Applications to partial differential equations, Science China Physics, Mechanics & Astronomy 68, 104704 (2025).
- [32] Z. Meng and Y. Yang, Geometric quantum encoding of a turbulent field (2025), arXiv:2508.05346.
- [33] Z.-X. Shang, N. Guo, D. An, and Q. Zhao, Designing a nearly optimal quantum algorithm for linear differential equations via lindbladians, Physical Review Letters **135**, 120604 (2025).
- [34] H. Su, S. Xiong, and Y. Yang, Efficient quantum state tomography with Chebyshev polynomials (2025), arXiv:2509.02112.
- [35] F. Tennie, S. Laizet, S. Lloyd, and L. Magri, Quantum computing for nonlinear differential equations and turbulence, Nature Reviews Physics 7, 220 (2025).
- [36] B. Wang, Z. Meng, Y. Zhao, and Y. Yang, Quantum lattice Boltzmann method for simulating nonlinear fluid dynamics (2025), arXiv:2502.16568.
- [37] Z. Wang, J. Zhong, K. Wang, Z. Zhu, Z. Bao, C. Zhu, W. Zhao, Y. Zhao, Y. Yang, C. Song, *et al.*, Simulating fluid vortex interactions on a superconducting quantum processor (2025), arXiv:2506.04023.
- [38] Y. Wang, R. Jiang, Y. Fan, X. Jia, J. Eisert, J. Liu, and J.-P. Liu, Towards efficient quantum algorithms for diffusion probability models (2025), arXiv:2502.14252.
- [39] G. Yang, A. Onwunta, and D. An, Quantum differential equation solvers with low state preparation cost: Eliminating the time dependence in dissipative equations, arXiv preprint arXiv:2508.15170 (2025).
- [40] B. Zhang, Z. Lu, Y. Zhao, and Y. Yang, Data-driven quantum Koopman method for simulating nonlinear dynamics (2025), arXiv:2507.21890.
- [41] C. Zhu, Z. Wang, S. Xiong, Y. Zhao, and Y. Yang, Quantum implicit representation of vortex filaments in turbulence (2025), arXiv:2502.18212.
- [42] D. Livescu, A. G. Nouri, F. Battaglia, and P. Givi, eds., *Modeling and Simulation of Turbulent Mixing and Reaction: For Power, Energy and Flight* (Springer, Germany, 2020).
- [43] Q. Wang, Towards high-fidelity aerospace design in the age of extreme scale supercomputing, in *AIAA* (2015).
- [44] T. Carleman, Application de la théorie des équations intégrales linéaires aux systèmes d'équations différentielles non linéaires, Acta Mathematica **59**, 63 (1932).
- [45] B. O. Koopman, Hamiltonian systems and transformation in hilbert space, Proceedings of the National Academy of Sciences 17, 315 (1931).
- [46] J. von Neumann, Zur operatorenmethode in der klassischen mechanik, Annals of Mathematics 33, 587 (1932).

- [47] M. Mohri, A. Rostamizadeh, and A. Talwalkar, Foundations of machine learning (MIT press, 2018).
- [48] S. Lloyd and L. Viola, Engineering quantum dynamics, Physical Review A 65, 010101 (2001).
- [49] C. Shen, K. Noh, V. V. Albert, S. Krastanov, M. H. Devoret, R. J. Schoelkopf, S. M. Girvin, and L. Jiang, Quantum channel construction with circuit quantum electrodynamics, Physical Review B 95, 10.1103/physrevb.95.134501 (2017).
- [50] W.-L. Ma, S. Puri, R. J. Schoelkopf, M. H. Devoret, S. M. Girvin, and L. Jiang, Quantum control of bosonic modes with superconducting circuits, Science Bulletin 66, 1789 (2021).
- [51] V. Giovannetti, S. Lloyd, and L. Maccone, Quantum random access memory, Physical review letters 100, 160501 (2008).
- [52] T. Tiecke, J. D. Thompson, N. P. de Leon, L. Liu, V. Vuletić, and M. D. Lukin, Nanophotonic quantum phase switch with a single atom, Nature 508, 241 (2014).
- [53] D. Leibfried, R. Blatt, C. Monroe, and D. Wineland, Quantum dynamics of single trapped ions, Reviews of Modern Physics 75, 281 (2003).
- [54] A. Signoles, A. Facon, D. Grosso, I. Dotsenko, S. Haroche, J.-M. Raimond, M. Brune, and S. Gleyzes, Confined quantum Zeno dynamics of a watched atomic arrow, Nature Physics 10, 715 (2014).
- [55] N. C. Menicucci, Fault-tolerant measurement-based quantum computing with continuous-variable cluster states, Physical review letters 112, 120504 (2014).
- [56] V. Havlíček, A. D. Córcoles, K. Temme, A. W. Harrow, A. Kandala, J. M. Chow, and J. M. Gambetta, Supervised learning with quantum-enhanced feature spaces, Nature 567, 209 (2019).
- [57] S. Succi, C. Sanavio, and P. Love, The foundational value of quantum computing for classical fluids (2025), arXiv:2510.09178.
- [58] R. Bellman, Introduction to matrix analysis (SIAM, 1997).
- [59] M. A. Nielsen and I. L. Chuang, Quantum Computation and Quantum Information: 10th Anniversary Edition (Cambridge University Press, Cambridge, 2010).
- [60] P. T. Cochrane, G. J. Milburn, and W. J. Munro, Macroscopically distinct quantum-superposition states as a bosonic code for amplitude damping, Physical Review A 59, 2631–2634 (1999).
- [61] E. Knill, R. Laflamme, and G. J. Milburn, A scheme for efficient quantum computation with linear optics, Nature 409, 46 (2001).
- [62] P. Leviant, Q. Xu, L. Jiang, and S. Rosenblum, Quantum capacity and codes for the bosonic loss-dephasing channel, Quantum 6, 821 (2022).
- [63] T. B. Harris, T. Matsuura, B. Q. Baragiola, and N. C. Menicucci, Logical channel for heralded and pure loss with the gottesmankitaev-preskill code, arXiv:2504.13497 (2025).
- [64] H.-P. Breuer and F. Petruccione, *The theory of open quantum systems* (Oxford University Press, Oxford, 2002).
- [65] A. J. Daley, Quantum trajectories and open many-body quantum systems, Adv. Phys. 63, 77 (2014).
- [66] K. Temme, S. Bravyi, and J. M. Gambetta, Error mitigation for short-depth quantum circuits, Phys. Rev. Lett. 119, 180509 (2017).
- [67] F. A. Mele, F. Salek, V. Giovannetti, and L. Lami, Quantum communication on the bosonic loss-dephasing channel, Phys. Rev. A 110, 012460 (2024).
- [68] H. M. Wiseman and G. J. Milburn, Quantum theory of optical feedback via homodyne detection, Phys. Rev. Lett. 70, 548 (1993)
- [69] I. Joseph, Koopman–von Neumann approach to quantum simulation of nonlinear classical dynamics, Phys. Rev. Research 2, 043102 (2020).

- [70] Y. T. Lin, R. B. Lowrie, D. Aslangil, Y. Subaşı, and A. T. Sorn-borger, Koopman von Neumann mechanics and the Koopman representation: A perspective on solving nonlinear dynamical systems with quantum computers (2022), arXiv:2202.02188.
- [71] I. Novikau and I. Joseph, Quantum algorithm for the advection—diffusion equation and the Koopman–von Neumann approach to nonlinear dynamical systems, Comput. Phys. Commun. 309, 109498 (2025).
- [72] H. Higuchi, Y. Ito, K. Sakamoto, K. Fujii, and A. Yoshikawa, A quantum algorithm for nonlinear electromagnetic fluid dynamics via Koopman–von Neumann linearization (2025), arXiv:2509.22503.
- [73] Y. Ito, Y. Tanaka, and K. Fujii, How to map linear differential equations to Schrödinger equations via carleman and Koopman-von Neumann embeddings for quantum algorithms (2023), arXiv:2311.15628.
- [74] D. Luo, J. Shen, R. Dangovski, and M. Soljačić, Quack: Accelerating gradient-based quantum optimization with Koopman operator learning, in *Advances in Neural Information Processing Systems*, Vol. 36 (2023) pp. 25662–25692.
- [75] Y. Tanaka and K. Fujii, A polynomial time quantum algorithm for exponentially large scale nonlinear differential equations via hamiltonian simulation (2023), arXiv:2305.00653.
- [76] U. Ghia, K. N. Ghia, and C. Shin, High-re solutions for incom-

- pressible flow using the navier-stokes equations and a multigrid method, Journal of computational physics **48**, 387 (1982).
- [77] M. Kiffner and D. Jaksch, Tensor network reduced order models for wall-bounded flows, Phys. Rev. Fluids 8, 124101 (2023).
- [78] R. J. Glauber, Coherent and incoherent states of the radiation field, Phys. Rev. **131**, 2766 (1963).
- [79] E. C. G. Sudarshan, Equivalence of semiclassical and quantum mechanical descriptions of statistical light beams, Phys. Rev. Lett. 10, 277 (1963).
- [80] D. Walls and G. J. Milburn, *Quantum Optics*, 3rd ed. (Springer, 2025).
- [81] C. W. Gardiner and P. Zoller, Quantum Noise: A Handbook of Markovian and Non-Markovian Quantum Stochastic Methods with Applications to Quantum Optics, 3rd ed. (Springer, Berlin Heidelberg, 2004).
- [82] H. J. Carmichael, Statistical Methods in Quantum Optics 1: Master Equations and Fokker-Planck Methods (Springer, Berlin Heidelberg, 1999).
- [83] N. G. van Kampen, *Stochastic Processes in Physics and Chemistry*, 3rd ed. (Elsevier, Amsterdam, 2007).
- [84] H. Haken, Laser Theory (Springer, Berlin Heidelberg, 1984).
- [85] M. O. Scully and M. S. Zubairy, *Quantum Optics* (Cambridge University Press, Cambridge, 1997).

### **Supplementary Materials**

#### **CONTENTS**

A. Technical derivations for the KvN formalism 1. Derivation of coherent-state operator identities	11 11
2. Recovering the classical ODE from the KvN lift	12
B. Quantum Channel Execution and Sampling Overhead	13
1. $Tr(A\rho)$ Calculation	13
2. Justification of the Stencil Radius Scaling: $R = \Theta(K)$	13
3. Proof of Theorem IV.2: Scaling of the Kraus Rank	14
C. Coherent-State Formalism in One Dimension	15
1. First-Order Moment Dynamics	16
2. 1D Burgers' Simulation	18
3. Extension to Two-Dimensional Lattices	20
D. Trotterization time-evolution algorithm for solving Lid-Driven Cavity Problem	22
E. Tensor Network Simulation of the Burgers' Equation	24
F. Open-System Dynamics in the <i>P</i> -Representation: Detailed Derivation	24

#### Appendix A: Technical derivations for the KvN formalism

#### 1. Derivation of coherent-state operator identities

In this subsection we prove Segal-Bargmann identities and for the purpose of the derivation, we adopt the unnormalized coherent state

$$|z\rangle = e^{z \, a^{\dagger}} |0\rangle, \qquad z \in \mathbb{C}.$$
 (A1)

We will repeatedly use the power-series expansion of the exponential and the definition/action of the Fock basis:

$$e^{z a^{\dagger}} = \sum_{n=0}^{\infty} \frac{z^n}{n!} \left( a^{\dagger} \right)^n, \tag{A2}$$

$$|n\rangle = \frac{(a^{\dagger})^n}{\sqrt{n!}} |0\rangle, \qquad a|n\rangle = \sqrt{n} |n-1\rangle.$$
 (A3)

Combining Eqs. (A1)-(A3), we can get the number-basis expansion of the coherent state:

$$|z\rangle = \sum_{n=0}^{\infty} \frac{z^n}{n!} (a^{\dagger})^n |0\rangle = \sum_{n=0}^{\infty} \frac{z^n}{\sqrt{n!}} \frac{(a^{\dagger})^n}{\sqrt{n!}} |0\rangle = \sum_{n=0}^{\infty} \frac{z^n}{\sqrt{n!}} |n\rangle.$$
 (A4)

Acting with a on Eq. (A4) and using  $a|n\rangle = \sqrt{n}|n-1\rangle$  from Eq. (A3), we obtain

$$a\left|z\right\rangle = \sum_{n=0}^{\infty} \frac{z^{n}}{\sqrt{n!}} \, a\left|n\right\rangle = \sum_{n=1}^{\infty} \frac{z^{n}}{\sqrt{n!}} \, \sqrt{n} \, \left|n-1\right\rangle \\ = \sum_{m=0}^{\infty} \frac{z^{m+1}}{\sqrt{m!}} \, \left|m\right\rangle = z \sum_{m=0}^{\infty} \frac{z^{m}}{\sqrt{m!}} \, \left|m\right\rangle = z \, \left|z\right\rangle,$$

which proves the first identity in Segal-Bargmann identities.

For the derivation of second equation in Segal–Bargmann identities, we can differentiate the definition (A1) term-by-term, it can yield:

$$\frac{\partial}{\partial z} |z\rangle = \sum_{n=1}^{\infty} \frac{nz^{n-1}}{n!} (a^{\dagger})^n |0\rangle = \sum_{m=0}^{\infty} \frac{z^m}{m!} (a^{\dagger})^{m+1} |0\rangle = a^{\dagger} |z\rangle \tag{A5}$$

#### 2. Recovering the classical ODE from the KvN lift

We assume the multivariable KvN setup in the main text:

$$\frac{d}{dt}z_j(t) = F_j(z(t), t), \qquad A(t) = \sum_{j=1}^n a_j^{\dagger} F_j(a, t),$$

with the coherent-state identities  $a_k \, |z\rangle = z_k \, |z\rangle$ ,  $F_j(a,t) \, |z\rangle = F_j(z,t) \, |z\rangle$ , and  $\langle z | \, a_j^\dagger = z_j^* \, \langle z |$  for the unnormalized product coherent state  $|z\rangle = \exp\left(\sum_\ell z_\ell a_\ell^\dagger\right) |0\rangle$ . Define

$$N_k(t) := \langle z(t) | a_k | z(t) \rangle, \ Z(t) := \langle z(t) | z(t) \rangle, \ z_k(t) = \frac{\langle z(t) | a_k | z(t) \rangle}{Z(t) := \langle z(t) | z(t) \rangle} = \frac{N_k(t)}{Z(t)}.$$

Differentiating the quotient term  $z_k(t)$  gives

$$\dot{z}_k = \frac{\dot{N}_k \, Z - N_k \, \dot{Z}}{Z^2}.$$

Using the lifted evolution from Eq. (1) and the conjugate transpose version  $\langle \dot{z}| = \langle z|A^{\dagger}$ , we get

$$\dot{N}_{k} = \langle \dot{z} | a_{k} | z \rangle + \langle z | a_{k} | \dot{z} \rangle = \langle z | A^{\dagger} a_{k} | z \rangle + \langle z | a_{k} A | z \rangle, \ \dot{Z} = \langle z | (A + A^{\dagger}) | z \rangle.$$

We now evaluate the matrix elements.

(i) For the term  $\langle z|\,a_kA\,|z\rangle$ , using  $[a_k,a_j^\dagger]=a_ka_j^\dagger-a_j^\dagger a_k=\delta_{kj}$  we can have

$$\langle z | a_k A | z \rangle = \sum_j \langle z | a_k a_j^{\dagger} F_j(a, t) | z \rangle = \sum_j \langle z | \left( a_j^{\dagger} a_k + \delta_{kj} \right) F_j(a, t) | z \rangle$$

$$= \sum_j \left( z_j^* z_k F_j(z, t) + \delta_{kj} F_j(z, t) \right) Z = \left( z_k \sum_j z_j^* F_j(z, t) + F_k(z, t) \right) Z.$$

(ii) For  $\langle z|A^{\dagger}a_k|z\rangle$ , writing  $A^{\dagger}=\sum_j F_j(a,t)^{\dagger}a_j$  and noting that  $F_j(a,t)^{\dagger}$  is a polynomial in creation operators, normal ordering gives

$$\langle z|F_j(a,t)^{\dagger}=F_j(z,t)^*\langle z|,$$

hence

$$\langle z|A^{\dagger}a_k|z\rangle = \sum_j \langle z|F_j(a,t)^{\dagger}a_ja_k|z\rangle = \sum_j F_j(z,t)^*\langle z|a_ja_k|z\rangle = z_k\sum_j z_jF_j(z,t)^*Z.$$

(iii) As for the normalization term, we have

$$\langle z|(A+A^{\dagger})|z\rangle = \sum_{j} \left(z_{j}^{*}F_{j}(z,t) + z_{j}F_{j}(z,t)^{*}\right)Z = 2\operatorname{Re}\sum_{j} z_{j}^{*}F_{j}(z,t)Z.$$

Collecting (i)-(iii), we have

$$\dot{z}_k = \frac{1}{Z} \left[ \langle z | a_k A | z \rangle + \langle z | A^{\dagger} a_k | z \rangle \right] - \frac{N_k}{Z^2} \langle z | (A + A^{\dagger}) | z \rangle$$

$$= \left( z_k \sum_j z_j^* F_j + F_k \right) + \left( z_k \sum_j z_j F_j^* \right) - z_k \cdot 2 \operatorname{Re} \sum_j z_j^* F_j$$

$$= F_k(z(t), t).$$

The terms proportional to  $z_k$  cancel exactly, leaving  $\dot{z}_k(t) = F_k(z(t), t)$ , which recovers the original ODE.

#### Appendix B: Quantum Channel Execution and Sampling Overhead

#### 1. $Tr(A\rho)$ Calculation

We aim to compute the value  $Tr(A\rho)$ , where A is the system generator. The derivation proceeds as follows:

$$\operatorname{Tr}(A\rho) = \operatorname{Tr}\left(A|z\rangle\langle z|\right) = \langle z|A|z\rangle$$

$$= \langle z|\frac{d}{dt}|z\rangle = \sum_{j} \langle z|a_{j}^{\dagger}F_{j}(z,t)|z\rangle$$

$$= \sum_{j} \langle z|a_{j}^{\dagger}|z\rangle \cdot F_{j}(z,t)$$

$$= \sum_{j} z_{j}^{*} \cdot F_{j}(z,t),$$

where the last step utilizes the well-known property of coherent states  $\langle z|\,a_j^\dagger\,|z\rangle=z_j^*$ , with  $z_j^*$  denoting the complex conjugate of  $z_j$ . This result follows from the fact that a coherent state  $|z\rangle$  is an eigenstate of the annihilation operator  $a_j$ , so the expectation value of the creation operator  $a_j^\dagger$  is the complex conjugate of the eigenvalue:  $a_j|z\rangle=z_j|z\rangle \Rightarrow \langle z|\,a_j^\dagger|z\rangle=z_j^*$ . Therefore, once the functions  $z_j(t)$  are determined, they can be substituted into  $F_j(z,t)$  to evaluate  $\mathrm{Tr}(A\rho)$ .

#### 2. Justification of the Stencil Radius Scaling: $R = \Theta(K)$

Here, we justify the scaling relation  $R = \Theta(K)$  for a compact finite-difference stencil on a uniform grid, where R is the Manhattan radius of the stencil and K is the order of the spatial derivative to be approximated. We establish this by proving a necessary lower bound and a constructive upper bound on R.

a. Necessity (Lower Bound). To show that R must grow at least linearly with K, we analyze the constraints required to construct a derivative stencil. Consider the simplest case: a one-dimensional, symmetric, centered stencil of radius R used to approximate the K-th derivative,  $f^{(K)}(x)$ . The approximation has the form:

$$D^{(K)}f(x) := \frac{1}{h^K} \sum_{m=-R}^{R} c_m f(x+mh) \approx f^{(K)}(x),$$
(B1)

where h is the grid spacing and  $\{c_m\}$  are the stencil coefficients, with  $c_{-m} = (-1)^K c_m$  for symmetry. To ensure accuracy, we expand f(x+mh) in a Taylor series around x:

$$D^{(K)}f(x) = \frac{1}{h^K} \sum_{m=-R}^{R} c_m \sum_{j=0}^{\infty} \frac{(mh)^j}{j!} f^{(j)}(x) = \sum_{j=0}^{\infty} \left(\frac{1}{j!} \sum_{m=-R}^{R} m^j c_m\right) f^{(j)}(x).$$
 (B2)

For this expression to approximate  $f^{(K)}(x)$ , the coefficients of the Taylor series must match. Specifically, the stencil must annihilate all lower-order derivative terms and correctly reproduce the K-th order term:

1. 
$$\sum_{m=-R}^{R} m^{j} c_{m} = 0$$
 for all  $j < K$ .

2. 
$$\sum_{m=-R}^{R} m^{K} c_{m} = K!$$
.

Due to the symmetry, conditions for j with parity different from K are automatically satisfied. This leaves approximately K/2 linear conditions from the first requirement, plus one condition from the second, for a total of  $\lceil K/2 \rceil + 1$  constraints. The number of independent variables we can choose is the number of unique coefficients, which is R+1 (i.e.,  $\{c_0, c_1, \ldots, c_R\}$ ). For a solution to exist, the number of variables must be at least the number of constraints:

$$R+1 > \lceil K/2 \rceil + 1 \implies R > \lceil K/2 \rceil.$$
 (B3)

This establishes the necessary lower bound  $R = \Omega(K)$ . This one-dimensional logic extends to higher dimensions by considering the stencil's restriction to any coordinate axis.

b. Sufficiency (Upper Bound). To show that R need not grow faster than linearly with K, we demonstrate that a solution can always be constructed. The system of linear equations for the coefficients  $\{c_m\}$  derived above is known to have a unique solution for  $R \ge \lceil K/2 \rceil$ . For any pure K-th derivative in one dimension, an explicit formula with the minimal radius  $R = \lceil K/2 \rceil$  can be found.

For mixed derivatives in d>2 dimensions, such as  $\partial^{p_1+\cdots+p_d}f/(\partial x_1^{p_1}\ldots\partial x_d^{p_d})$  where  $\sum p_i=K$ , we can construct the full stencil by composing 1D stencils along each axis. The 1D stencil for the  $p_i$ -th derivative has a radius of  $\lceil p_i/2 \rceil$ . The total Manhattan radius of the composite stencil is the sum of the individual radii:

$$R = \sum_{i=1}^{d} \lceil p_i / 2 \rceil \le \sum_{i=1}^{d} (p_i / 2 + 1) = \frac{K}{2} + d.$$
 (B4)

For fixed dimension d, this shows R is bounded by a linear function of K, establishing the upper bound  $R = \mathcal{O}(K)$ .

c. Conclusion and Example. Combining the lower bound  $R = \Omega(K)$  and the upper bound  $R = \mathcal{O}(K)$ , we conclude that the stencil radius must scale linearly with the derivative order:  $R = \Theta(K)$ .

Worked Example (K = 4 in 1D): To approximate  $f^{(4)}(x)$ , the minimal radius is  $R = \lceil 4/2 \rceil = 2$ . We seek coefficients for the 5-point stencil  $\{-2, -1, 0, 1, 2\}$ . The constraints are:

- $c_0 + 2c_1 + 2c_2 = 0$  (to kill f(x) term, i.e., j = 0)
- $2c_1 + 8c_2 = 0$  (to kill f''(x) term, i.e., j = 2)
- $2c_1 + 32c_2 = 4! = 24$  (to match  $f^{(4)}(x)$  term, i.e., j = 4)

Solving this system yields  $c_2 = 1$ ,  $c_1 = -4$ , and  $c_0 = 6$ . This gives the well-known 5-point stencil for the fourth derivative:

$$f^{(4)}(x) \approx \frac{f(x-2h) - 4f(x-h) + 6f(x) - 4f(x+h) + f(x+2h)}{h^4}.$$
 (B5)

This achieves the minimal radius R=2 for K=4, consistent with R=K/2.

d. Connection to Standard Stencils in 2D and 3D. The linear relationship  $R = \Theta(K)$  is consistent with stencils commonly used in computational physics. For instance, the advection operator (K=1) is discretized with first differences, requiring a nearest-neighbor stencil (R=1). The diffusion operator or Laplacian (K=2) is often approximated with a 5-point (in 2D) or 7-point (in 3D) stencil, which also only involves nearest neighbors (R=1). More complex operators like the bi-Laplacian (K=4) require a wider 13-point stencil that includes nodes up to two grid points away, giving a radius of R=2. In all these standard cases, the radius R is approximately K/2, validating the formal scaling relationship.

#### 3. Proof of Theorem IV.2: Scaling of the Kraus Rank

This section provides the proof for the scaling of the total Kraus rank, N, which determines the per-step circuit depth of the algorithm. The theorem states that for a system with L grid points, a nonlinearity of degree r, and a stencil of order K, the Kraus rank scales as  $N = \mathcal{O}(LK^{dr})$ .

a. Premise: Structure of the Generator. The evolution generator A is a sum of local terms over all grid points i:  $A = \sum_{i,\alpha} L_{i,\alpha}$ . As defined in the main text, each term  $L_{i,\alpha}$  corresponds to a distinct normal-ordered monomial representing a component of the PDE's dynamics. For a nonlinearity of degree r, each monomial has the form:

$$L_{i,\alpha} = a_i^{\dagger} \prod_{m=1}^r a_{j_m^{(\alpha)}}, \tag{B6}$$

where the annihilation operators  $a_{j_m^{(\alpha)}}$  act on grid points within the local neighborhood  $N_R(i)$  of grid point i. The index  $\alpha$  enumerates every unique combination of these r annihilation operators. The proof proceeds by counting the number of these unique monomials.

b. Step 1: Counting Monomials per grid point. For a fixed grid point i, we need to determine how many unique monomials  $L_{i,\alpha}$  can be constructed. This is equivalent to counting the number of distinct products of r annihilation operators,  $\prod_{m=1}^r a_{j_m}$ , where each index  $j_m$  is chosen from the set of neighbors  $N_R(i)$ .

Let S be the number of selectable neighbors in the stencil (excluding the center grid point i), and let  $S_{\rm eff}$  be the effective number of choices, where  $S_{\rm eff} = S + 1$  if self-coupling (terms like  $a_i^r$ ) is allowed, and  $S_{\rm eff} = S$  otherwise. Because the annihilation operators are bosonic, they commute  $(a_j a_k = a_k a_j)$ , so the order in which we choose the neighbors does not matter. Furthermore, we are allowed to choose the same neighbor multiple times (e.g.,  $a_k^2$ ).

This is a classic combinatorial problem: counting the number of multisets of size r drawn from a set of size  $S_{\text{eff}}$ . The number of such combinations is given by the multiset coefficient:

$$\#\{\alpha \text{ at grid point } i\} = {S_{\text{eff}} + r - 1 \choose r}.$$
 (B7)

c. Step 2: Total Kraus Rank Scaling. The total number of distinct local monomials over the entire lattice is the number of grid points, L, multiplied by the number of monomials per grid point. By the theorem's assumption, each unique monomial corresponds to a constant number,  $c_r = \mathcal{O}(1)$ , of non-identity Kraus operators. Therefore, the total Kraus rank N is:

$$N = c_r \cdot L \cdot \binom{S_{\text{eff}} + r - 1}{r}.$$
 (B8)

For the purpose of asymptotic scaling, we are interested in the behavior for large stencils ( $S_{\text{eff}} \gg r$ ). The binomial coefficient can be approximated by a polynomial:

$$\binom{S_{\text{eff}} + r - 1}{r} = \frac{(S_{\text{eff}} + r - 1)\dots(S_{\text{eff}})}{r!} = \mathcal{O}(S_{\text{eff}}^r).$$
 (B9)

Thus, the Kraus rank scales as  $N = \mathcal{O}(L \cdot S_{\text{eff}}^r)$ .

d. Step 3: Final Expression in Terms of Physical Parameters. To complete the proof, we express  $S_{\text{eff}}$  in terms of the physical parameters d (dimension) and K (derivative order). The number of grid points in a stencil of Manhattan radius R in d dimensions scales as  $S = \Theta(R^d)$ . Since  $S_{\text{eff}}$  is dominated by S, it follows that  $S_{\text{eff}} = \Theta(R^d)$ .

From the analysis in Supplementary Materials B 2, we have the established relationship  $R = \Theta(K)$ . Substituting this into our expression for  $S_{\text{eff}}$  gives:

$$S_{\text{eff}} = \Theta(K^d). \tag{B10}$$

Finally, substituting this into our scaling law for N yields the main result:

$$N = \mathcal{O}(L \cdot S_{\text{eff}}^r) = \mathcal{O}(L \cdot (K^d)^r) = \mathcal{O}(LK^{dr}). \tag{B11}$$

This confirms the scaling of the Kraus rank as stated in Theorem IV.2. The per-step circuit depth, implemented via a binary-tree architecture, scales logarithmically with the rank, giving Depth  $= \mathcal{O}(\log N) = \mathcal{O}(\log L + dr \log K)$ .

#### Appendix C: Coherent-State Formalism in One Dimension

For a single bosonic mode with annihilation operator a, the coherent state  $|z\rangle$  is defined by

$$a|z\rangle = z|z\rangle, \qquad \langle z|a^{\dagger} = z^* \langle z|, \qquad \langle a\rangle = \langle z|a|z\rangle = z,$$
 (C1)

where  $z \in \mathbb{C}$  is the coherent amplitude and  $z^*$  denotes its complex conjugate. In the multimode setting with annihilation operators  $\{a_j\}_{j=1}^n$ , we define the classical field amplitude at time t by

$$z_j(t) := \text{Tr}[a_j \rho(t)] = \langle a_j \rangle_t, \tag{C2}$$

and, for any normal-ordered polynomial  $G(a^{\dagger}, a)$ , we use the coherent-state rule  $\langle z | G(a^{\dagger}, a) | z \rangle = G(z^*, z)$ .

We describe the short-time dynamics by the normal-ordered operator

$$M = \sum_{k=1}^{n} a_k^{\dagger} F_k(a_1, \dots, a_n),$$
 (C3)

which generates the raw update

$$\rho_{\text{raw}}(t + \Delta t) = e^{M\Delta t} \, \rho(t) \, e^{M^{\dagger} \Delta t}. \tag{C4}$$

Since  $e^{M\Delta t}$  is not generally an isometry (as M need not be anti-Hermitian), the state must be renormalized:

$$\mathcal{N}(t + \Delta t) = \text{Tr}[\rho_{\text{raw}}(t + \Delta t)], \qquad \rho(t + \Delta t) = \frac{\rho_{\text{raw}}(t + \Delta t)}{\mathcal{N}(t + \Delta t)}.$$
 (C5)

Equivalently, for any observable O,

$$\langle O \rangle_{t+\Delta t} = \frac{\text{Tr}\left[e^{M^{\dagger} \Delta t} O e^{M \Delta t} \rho(t)\right]}{\text{Tr}\left[e^{M^{\dagger} \Delta t} e^{M \Delta t} \rho(t)\right]}.$$
 (C6)

#### 1. First-Order Moment Dynamics

a. Mean Update: Forward Euler

To obtain the first-order expansion of the mean field, let  $|z\rangle$  denote a product of coherent states with amplitudes  $z_k = \langle a_k \rangle_t$ , and define the shorthand

$$\Sigma(z) := \sum_{k=1}^{n} z_k^* F_k(z). \tag{C7}$$

Expanding Eq. (C6) with  $O = a_i$  yields

$$\langle a_j \rangle_{t+\Delta t} = \frac{\langle z | (1 + M^{\dagger} \Delta t) a_j (1 + M \Delta t) | z \rangle}{\langle z | (1 + M^{\dagger} \Delta t) (1 + M \Delta t) | z \rangle} + O(\Delta t^2).$$
 (C8)

The relevant coherent-state matrix elements are

$$\langle z|a_jM|z\rangle = F_j(z) + z_j\Sigma(z), \qquad \langle z|M^{\dagger}a_j|z\rangle = z_j\Sigma(z)^*,$$
 (C9)

$$\langle z | M | z \rangle = \Sigma(z), \qquad \langle z | M^{\dagger} | z \rangle = \Sigma(z)^*,$$
 (C10)

so that the denominator evaluates to

Den = 
$$\langle z | (1 + M^{\dagger} \Delta t + M \Delta t + O(\Delta t^{2})) | z \rangle$$
  
=  $1 + \Delta t (\langle z | M^{\dagger} | z \rangle + \langle z | M | z \rangle) + O(\Delta t^{2}))$   
=  $1 + \Delta t (\Sigma(z)^{*} + \Sigma(z)) + O(\Delta t^{2}))$   
=  $1 + 2\Delta t \operatorname{Re} \Sigma(z) + O(\Delta t^{2}).$  (C11)

Similarly, we expand the numerator to first order:

$$\operatorname{Num} = \langle z | (1 + M^{\dagger} \Delta t) a_{j} (1 + M \Delta t) | z \rangle$$

$$= \langle z | (a_{j} + a_{j} M \Delta t + M^{\dagger} a_{j} \Delta t + O(\Delta t^{2})) | z \rangle$$

$$= \langle z | a_{j} | z \rangle + \Delta t (\langle z | a_{j} M | z \rangle + \langle z | M^{\dagger} a_{j} | z \rangle) + O(\Delta t^{2}).$$
(C12)

Substituting the matrix elements from Eq. (C10) simplifies the numerator to:

$$\operatorname{Num} = z_j + \Delta t(F_j(z) + z_j \Sigma(z) + z_j \Sigma(z)^*) + O(\Delta t^2)$$

$$= z_j + \Delta t F_j(z) + 2\Delta t z_j \operatorname{Re} \Sigma(z) + O(\Delta t^2)$$
(C13)

With both terms expanded, we can now evaluate the full fraction:

$$\langle a_j \rangle_{t+\Delta t} = \frac{z_j + \Delta t F_j(z) + 2\Delta t z_j \operatorname{Re} \Sigma(z)}{1 + 2\Delta t \operatorname{Re} \Sigma(z)} + O(\Delta t^2)$$
 (C14)

To resolve this, we use the first-order Taylor approximation  $\frac{1}{1+x} \approx 1 - x$  for small value  $x = 2\Delta t \operatorname{Re} \Sigma(z)$ . This turns the division into a multiplication:

$$\langle a_j \rangle_{t+\Delta t} = (z_j + \Delta t F_j(z) + 2\Delta t z_j \operatorname{Re} \Sigma(z)) (1 - 2\Delta t \operatorname{Re} \Sigma(z)) + O(\Delta t^2)$$

$$= z_j + \Delta t F_j(z) + 2\Delta t z_j \operatorname{Re} \Sigma(z) - z_j \cdot 2\Delta t \operatorname{Re} \Sigma(z) + O(\Delta t^2)$$

$$= z_j + \Delta t F_j(z) + O(\Delta t^2)$$
(C15)

Therefore,

$$z_j(t + \Delta t) = z_j(t) + \Delta t F_j(z(t)) + O(\Delta t^2), \qquad \text{(forward Euler step)}$$
 (C16)

which identifies the coherent amplitude with the classical Euler update rule. By definition,

$$z_i(t + \Delta t) = \text{Tr}[a_i \rho(t + \Delta t)]. \tag{C17}$$

b. Variance Update: First Order

We next turn to fluctuations around the coherent amplitude. Define the annihilation-operator variance at grid point j:

$$\operatorname{Var}_{j}(t) := \operatorname{Var}(a_{j}) = \langle a_{j}^{\dagger} a_{j} \rangle_{t} - \left| \langle a_{j} \rangle_{t} \right|^{2} = \langle (a_{j} - z_{j}(t))^{\dagger} (a_{j} - z_{j}(t)) \rangle_{t}. \tag{C18}$$

Using Eq. (C6), introduce the shorthand

$$E_1 = \langle e^{M^{\dagger} \Delta t} a_j e^{M \Delta t} \rangle_t, \qquad E_2 = \langle e^{M^{\dagger} \Delta t} a_j^{\dagger} a_j e^{M \Delta t} \rangle_t, \qquad D = \langle e^{M^{\dagger} \Delta t} e^{M \Delta t} \rangle_t,$$

so that, consistently with (C18),

$$\langle a_j \rangle_{t+\Delta t} = \frac{E_1}{D}, \qquad \langle a_j^{\dagger} a_j \rangle_{t+\Delta t} = \frac{E_2}{D}, \qquad V_j(t+\Delta t) = \frac{E_2 D - |E_1|^2}{D^2}.$$

Expanding each quantity to first order in  $\Delta t$  gives

$$E_{1} = \langle e^{M^{\dagger} \Delta t} a_{j} e^{M \Delta t} \rangle_{t} = \langle (1 + \Delta t M^{\dagger}) a_{j} (1 + \Delta t M) \rangle_{t} + O(\Delta t^{2})$$

$$= \langle a_{j} \rangle_{t} + \Delta t \langle M^{\dagger} a_{j} + a_{j} M \rangle_{t} + O(\Delta t^{2}) = z_{j} + \Delta t A_{1} + O(\Delta t^{2}), \tag{C19}$$

with

$$A_1 := \langle M^{\dagger} a_j + a_j M \rangle_t. \tag{C20}$$

Similarly,

$$E_{2} = \langle e^{M^{\dagger} \Delta t} a_{j}^{\dagger} a_{j} e^{M \Delta t} \rangle_{t} = \langle (1 + \Delta t M^{\dagger}) a_{j}^{\dagger} a_{j} (1 + \Delta t M) \rangle_{t} + O(\Delta t^{2})$$

$$= \langle a_{j}^{\dagger} a_{j} \rangle_{t} + \Delta t \langle M^{\dagger} a_{j}^{\dagger} a_{j} + a_{j}^{\dagger} a_{j} M \rangle_{t} + O(\Delta t^{2}) = (V_{j}(t) + |z_{j}|^{2}) + \Delta t A_{2} + O(\Delta t^{2}), \tag{C21}$$

with

$$A_2 := \langle M^{\dagger} a_j^{\dagger} a_j + a_j^{\dagger} a_j M \rangle_t. \tag{C22}$$

For the normalization factor,

$$D = \langle e^{M^{\dagger} \Delta t} e^{M \Delta t} \rangle_{t} = \langle (1 + \Delta t M^{\dagger}) (1 + \Delta t M) \rangle_{t} + O(\Delta t^{2})$$
  
= 1 + \Delta t (\langle M \rangle\_{t} + \langle M^{\dagger} \rangle\_{t}) + O(\Delta t^{2}) = 1 + \Delta t S + O(\Delta t^{2}), (C23)

where

$$S := \langle M \rangle_t + \langle M^{\dagger} \rangle_t. \tag{C24}$$

Collecting the three expansions,

$$E_1 = z_j + \Delta t A_1 + O(\Delta t^2), \qquad E_2 = |z_j|^2 + V_j(t) + \Delta t A_2 + O(\Delta t^2), \qquad D = 1 + \Delta t S + O(\Delta t^2).$$

The coefficients are obtained from coherent–state matrix elements of  $M=\sum_k a_k^{\dagger} F_k(a)$ :

$$A_1 = F_j(z) + z_j \Sigma(z) + z_j \Sigma(z)^*, \qquad A_2 = |z_j|^2 (\Sigma + \Sigma^*) + z_j^* F_j(z) + z_j F_j(z)^*, \qquad S = \Sigma + \Sigma^*,$$

where

$$\Sigma(z) := \sum_{k} z_{k}^{*} F_{k}(z).$$

For notational simplicity, let  $z \equiv z_i$  and  $\Sigma \equiv \Sigma(z)$ . Using these definitions,

$$A_2 + S|z|^2 - (z^*A_1 + zA_1^*) = 0,$$

2 1D Burgers' Simulation 18

as shown earlier. Hence the numerator obeys

$$E_{2}D - |E_{1}|^{2} = \left( \langle a_{j}^{\dagger} a_{j} \rangle_{t} - |\langle a_{j} \rangle_{t}|^{2} \right) + \Delta t \left( A_{2} + S \langle a_{j}^{\dagger} a_{j} \rangle_{t} - (z^{*} A_{1} + z A_{1}^{*}) \right) + O(\Delta t^{2})$$

$$= \operatorname{Var}_{j}(t) + \Delta t \left( A_{2} + S|z|^{2} - (z^{*} A_{1} + z A_{1}^{*}) \right) + \Delta t S \operatorname{Var}_{j}(t) + O(\Delta t^{2})$$

$$= \operatorname{Var}_{j}(t) + \Delta t S \operatorname{Var}_{j}(t) + O(\Delta t^{2})$$

$$= \operatorname{Var}_{j}(t) (1 + \Delta t S) + O(\Delta t^{2}).$$
(C25)

Since  $D^2 = (1 + \Delta t S)^2 = 1 + 2\Delta t S + O(\Delta t^2)$ , we obtain the variance update

$$\operatorname{Var}_{j}(t + \Delta t) = \frac{E_{2}D - |E_{1}|^{2}}{D^{2}} = \frac{\operatorname{Var}_{j}(t)(1 + \Delta tS) + O(\Delta t^{2})}{(1 + \Delta tS)^{2}}$$

$$= \frac{\operatorname{Var}_{j}(t)(1 + \Delta tS)}{(1 + \Delta tS)^{2}} + \frac{O(\Delta t^{2})}{(1 + \Delta tS)^{2}}$$

$$= \frac{\operatorname{Var}_{j}(t)}{1 + \Delta tS} + O(\Delta t^{2})$$

$$= \operatorname{Var}_{j}(t)(1 - \Delta tS + O(\Delta t^{2})) + O(\Delta t^{2})$$

$$= (1 - 2\Delta t \operatorname{Re} \Sigma(z(t))) \operatorname{Var}_{j}(t) + O(\Delta t^{2}).$$
(C26)

In particular, if  $\operatorname{Var}_j(t) = 0$  (e.g., a product of coherent states at time t), then  $\operatorname{Var}_j(t + \Delta t) = O(\Delta t^2)$ . More generally, we can write:

$$\operatorname{Var}_{i}(t + \Delta t) = (1 - 2\Delta t \operatorname{Re}\Sigma(z(t))) \operatorname{Var}_{i}(t) + O(\Delta t^{2}), \text{ and if } \operatorname{Var}_{i}(t) = 0, \operatorname{Var}_{i}(t + \Delta t) = O(\Delta t^{2}).$$
 (C27)

#### 2. 1D Burgers' Simulation

Consider the semi-discrete 1D viscous Burgers update with Reynolds number  $\mathcal{R}_e$ 

$$\frac{\partial u}{\partial t} = -u \frac{\partial u}{\partial x} + \frac{1}{R_e} \frac{\partial^2 u}{\partial x^2}.$$
 (C28)

For the semi-discrete 1D viscous Burgers step with grid spacing  $\Delta x$ , the stencil is

$$F_k(z) = \frac{z_{k+1} - 2z_k + z_{k-1}}{R_e \Delta x^2} - \frac{z_k}{2\Delta x} (z_{k+1} - z_{k-1}).$$
 (C29)

The first term diffusive contribution corresponds to the linear local operator which is nearest-neighbor in d=1. Thus  $|E|\approx 2L$ , N=4L, and the per-step depth is  $\mathcal{O}(\log L)$ . We use the generator of the form

$$A = \sum_{k} a_{k}^{\dagger} F_{k}(a), \qquad F_{k}(a) = \underbrace{\frac{a_{k+1} - 2a_{k} + a_{k-1}}{R_{e} \Delta x^{2}}}_{\text{diffusion}} - \underbrace{\frac{a_{k}}{2\Delta x} (a_{k+1} - a_{k-1})}_{\text{convection}}.$$
 (C30)

For a product coherent state  $|z\rangle$  at time t, write  $z_k:=\langle a_k\rangle_t$ . By normal ordering,  $F_k(z)$  is obtained by substitution  $a_\ell\mapsto z_\ell$ :

$$F_k(z) = \frac{z_{k+1} - 2z_k + z_{k-1}}{R_e \Delta x^2} - \frac{z_k}{2\Delta x} (z_{k+1} - z_{k-1}).$$
 (C31)

The overlap  $\Sigma(z) := \sum_{\ell} z_{\ell}^* F_{\ell}(z)$  then splits into diffusion and convection pieces,

$$\Sigma(z) = \Sigma_{\text{diff}}(z) + \Sigma_{\text{conv}}(z) = \sum_{k} \frac{z_k^*(z_{k+1} - 2z_k + z_{k-1})}{R_e \Delta x^2} - \sum_{k} \frac{|z_k|^2}{2\Delta x} (z_{k+1} - z_{k-1}).$$
 (C32)

a. Forward-Euler mean update. By Eq. (C16) we have, for each grid point k,

$$z_k(t + \Delta t) = z_k(t) + F_k(z(t)) \Delta t + O(\Delta t^2), \qquad F_k(z) \text{ given by (C31)}.$$
 (C33)

b. First order variance. Specializing the first-order coefficients in Sec. C to the Burgers generator (C30) gives

$$A_1^{(k)} = \langle M^{\dagger} a_k + a_k M \rangle_t = F_k(z) + z_k \Sigma(z) + z_k \Sigma(z)^*, \qquad S = \langle M \rangle_t + \langle M^{\dagger} \rangle_t = \Sigma(z) + \Sigma(z)^*, \tag{C34}$$

and

$$A_2^{(k)} = \langle M^{\dagger} a_k^{\dagger} a_k + a_k^{\dagger} a_k M \rangle_t = |z_k|^2 (\Sigma(z) + \Sigma(z)^*) + z_k^* F_k(z) + z_k F_k(z)^*. \tag{C35}$$

Inserting these into  $V_k(t+\Delta t)=\frac{E_2D-|E_1|^2}{D^2}$  with the expansions  $E_1=z_k+\Delta t A_1^{(k)}+O(\Delta t^2)$ ,  $E_2=|z_k|^2+V_k(t)+\Delta t A_2^{(k)}+O(\Delta t^2)$ ,  $D=1+\Delta t S+O(\Delta t^2)$ , the  $O(\Delta t)$  term cancels identically (Sec. C), and therefore

$$\operatorname{Var}(a_k)_{t+\Delta t} = \operatorname{Var}(a_k)_t + O(\Delta t^2). \tag{C36}$$

In particular, starting from a product of coherent states,  $Var(a_k)_t = 0$  remains zero to first order.

c. Analysis of Numerical Stability. Write forward differences  $\delta^+ z_k := z_{k+1} - z_k$  and the discrete Laplacian  $\Delta z_k := z_{k+1} - 2z_k + z_{k-1} = \delta^+ z_k - \delta^+ z_{k-1}$ . Under periodic boundary conditions, a discrete summation by parts gives

$$\sum_{k} z_{k}^{*} \Delta z_{k} = \sum_{k} z_{k}^{*} (\delta^{+} z_{k} - \delta^{+} z_{k-1}) = \sum_{k} z_{k}^{*} \delta^{+} z_{k} - \sum_{k} z_{k+1}^{*} \delta^{+} z_{k} = -\sum_{k} \delta^{+} z_{k}^{*} \delta^{+} z_{k}. = -\sum_{k} \left| \delta^{+} z_{k} \right|^{2}$$
(C37)

Hence the diffusive part satisfies

$$\operatorname{Re} \Sigma_{\operatorname{diff}}(z) = \frac{1}{R_e \Delta x^2} \operatorname{Re} \sum_{k} z_k^* \Delta z_k = -\frac{1}{R_e \Delta x^2} \sum_{k} \left| \delta^+ z_k \right|^2 \le 0, \tag{C38}$$

which is strictly dissipative (negative semidefinite).

For the convection contribution,

$$\Sigma_{\text{conv}}(z) = -\frac{1}{2\Delta x} \sum_{k} |z_{k}|^{2} (z_{k+1} - z_{k-1}).$$
 (C39)

If the coherent amplitudes are chosen globally real (fixing a global phase),  $\Sigma_{\text{conv}}(z)$  is real but does not have a definite sign in general. Nevertheless it can be bounded in terms of the discrete gradient:

$$\left| \Sigma_{\text{conv}}(z) \right| \leq \frac{1}{2\Delta x} \sum_{k} |z_{k}|^{2} \left( |\delta^{+}z_{k}| + |\delta^{+}z_{k-1}| \right) \leq \frac{\|z\|_{\infty}^{2}}{\Delta x} \sum_{k} |\delta^{+}z_{k}| \leq \frac{\epsilon}{R_{e} \Delta x^{2}} \sum_{k} |\delta^{+}z_{k}|^{2} + \frac{R_{e} \Delta x^{2}}{4\epsilon} \|z\|_{\infty}^{4} L, \quad (C40)$$

for any  $\epsilon > 0$  (by Young's inequality), where L is the number of grid points and  $||z||_{\infty} := \max_k |z_k|$ . Combining (C38)–(C40) shows that for sufficiently diffusive regimes (small  $R_e$  or adequately resolved grids), the dissipative term dominates  $\operatorname{Re}\Sigma(z)$ , ensuring stability of the normalized update; in practice this manifests as a controlled denominator  $1 + 2\Delta t \operatorname{Re}\Sigma(z)$  in Eq. (C6).

d. Summary for the Burgers step. Given  $F_k(z)$  in (C31) and  $\Sigma(z)$  in (C32), the one-step evolution obeys

$$z_k(t + \Delta t) = z_k(t) + \Delta t F_k(z(t)) + O(\Delta t^2), \qquad \operatorname{Var}(a_k)_{t+\Delta t} = \operatorname{Var}(a_k)_t + O(\Delta t^2), \tag{C41}$$

with the diffusive part contributing a strictly nonpositive  $\operatorname{Re} \Sigma_{\operatorname{diff}}(z)$  by (C38), and the convective part controlled by (C40). In the common gauge where all  $z_k$  are real, the identity  $\sum_k z_k \, \Delta z_k = -\sum_k (\delta^+ z_k)^2 \leq 0$  makes the stabilizing role of diffusion explicit.

e. Numerical results for the Burgers' equation. For each grid point j, define the coherent amplitude as  $z_j(t) := \text{Tr}[a_j \rho(t)]$  and the variance  $\text{Var}_j(t) := \text{Var}(a_j)_t = \langle a_j^\dagger a_j \rangle_t - \left| \langle a_j \rangle_t \right|^2$ . With the short-time generator expressed in normal order as  $A = \sum_k a_k^\dagger F_k(a)$ , the coherent-state algebra (Supplementary Materials C) yields the following update formulae

$$z_i(t + \Delta t) = z_i(t) + \Delta t F_i(z) + \mathcal{O}(\Delta t^2), \tag{C42}$$

$$Var_{i}(t + \Delta t) = Var_{i}(t) + \mathcal{O}(\Delta t^{2}). \tag{C43}$$

The cancellation of all  $\mathcal{O}(\Delta t)$  contributions in Eq. (C43) is nontrivial. Substituting the coherent-state expansions for the first and second moments into  $\mathrm{Var}_j = (E_2 D - |E_1|^2)/D^2$  shows that the terms proportional to  $\Delta t$  cancel exactly (Supplementary Materials C36), leaving only  $\mathcal{O}(\Delta t^2)$  corrections.

For reference, we use the continuous 1D viscous Burgers' equation as shown in Eq. (C28) with its stencil, Eq. (C29). Under this discretization, the coherent amplitudes advance by the update in Eq. (C42), reproducing nonlinear steepening and diffusion, while variances remain constant to first order.

Fig. 3 illustrates the temporal evolution of the mean profile and its associated bias. The initial distribution travels to the right, becoming asymmetric due to nonlinearity and developing a shock, while the error remains small. Table I demonstrates the estimates of the variance from  $N=10^4$  samples per grid point match the analytic prediction within the expected  $\sqrt{2/(N-1)}$  envelope.

#### 3. Extension to Two-Dimensional Lattices

The generator of the short-time dynamics now takes the form:

$$A = \sum_{p',q'} a_{p',q'}^{\dagger} F_{p',q'}(a), \tag{C44}$$

where  $F_{p',q'}(a)$  is a function of all annihilation operators  $\{a_{p',q'}\}$  on the lattice. The overlap scalar  $\Sigma(z)$  is also a double summation:

$$\Sigma(z) := \sum_{p',q'} z_{p',q'}^* F_{p',q'}(z). \tag{C45}$$

a. Mean-Field Evolution. To find the first-order evolution of the mean field  $z_{p,q}$ , we expand the expectation value of the operator  $O = a_{p,q}$ :

$$\langle a_{p,q} \rangle_{t+\Delta t} = \frac{\langle z | (1 + M^{\dagger} \Delta t) a_{p,q} (1 + M \Delta t) | z \rangle}{\langle z | (1 + M^{\dagger} \Delta t) (1 + M \Delta t) | z \rangle} + O(\Delta t^2). \tag{C46}$$

The algebraic structure of the operator commutation relations is unchanged, so the coherent-state matrix elements are direct analogues of the 1D case:

$$\langle z|a_{p,q}M|z\rangle = F_{p,q}(z) + z_{p,q}\Sigma(z), \qquad \langle z|M^{\dagger}a_{p,q}|z\rangle = z_{p,q}\Sigma(z)^*,$$
 (C47)

$$\langle z|M|z\rangle = \Sigma(z), \qquad \langle z|M^{\dagger}|z\rangle = \Sigma(z)^*.$$
 (C48)

Thus the denominator is

$$Den = 1 + 2\Delta t \operatorname{Re}\Sigma(z) + O(\Delta t^2), \tag{C49}$$

and the numerator is

$$Num = z_{p,q} + \Delta t F_{p,q}(z) + 2\Delta t z_{p,q} \operatorname{Re} \Sigma(z) + O(\Delta t^2).$$
 (C50)

When combined, the terms involving  $\operatorname{Re}\Sigma(z)$  cancel identically, leaving the forward Euler update:

$$z_{p,q}(t + \Delta t) = z_{p,q}(t) + \Delta t F_{p,q}(z(t)) + O(\Delta t^2).$$
 (C51)

b. First-Order Variance Evolution. Consider the variance of the annihilation operator at grid point (p,q):

$$\operatorname{Var}_{p,q}(t) := \operatorname{Var}(a_{p,q}) = \left\langle a_{p,q}^{\dagger} a_{p,q} \right\rangle_t - \left| \left\langle a_{p,q} \right\rangle_t \right|^2. \tag{C52}$$

The variance update is again

$$\operatorname{Var}_{p,q}(t + \Delta t) = \frac{E_2 D - |E_1|^2}{D^2},$$

with  $E_1$ ,  $E_2$ , D defined analogously to the 1D case.

The key identity

$$A_2^{(p,q)} + S|z_{p,q}|^2 - \left(z_{p,q}^* A_1^{(p,q)} + z_{p,q} (A_1^{(p,q)})^*\right) = 0$$
 (C53)

holds in 2D just as in 1D, since it is purely algebraic and does not depend on the lattice dimension. Therefore the numerator reduces to

$$E_2D - |E_1|^2 = \operatorname{Var}_{p,q}(t) (1 + \Delta t S) + O(\Delta t^2),$$

and dividing by  $D^2 = (1 + \Delta t S)^2$  gives

$$\operatorname{Var}_{p,q}(t + \Delta t) = (1 - 2\Delta t \operatorname{Re} \Sigma(z)) \operatorname{Var}_{p,q}(t) + O(\Delta t^{2}). \tag{C54}$$

In particular, if  $\operatorname{Var}_{p,q}(t) = 0$  (a product of coherent states), then  $\operatorname{Var}_{p,q}(t + \Delta t) = O(\Delta t^2)$ .

a. 2D Fisher-KPP Simulation

Consider the short-time generator on a 2D lattice

$$A = \sum_{i,j} a_{i,j}^{\dagger} F_{i,j}(a), \qquad \Sigma(z) := \sum_{i,j} z_{i,j}^{*} F_{i,j}(z), \tag{C55}$$

with the grid point-wise first-order update from Sec. C3:

$$z_{i,j}(t+\Delta t) = z_{i,j}(t) + \Delta t F_{i,j}(z(t)) + O(\Delta t^2). \tag{C56}$$

We take the (discrete) Fisher-type advection-diffusion-reaction form

$$F_{i,j}(a) = \underbrace{\frac{y_j}{2\Delta x} \left( \frac{a_{i+1,j}}{\sqrt{x_{i+1}^2 + y_j^2}} - \frac{a_{i-1,j}}{\sqrt{x_{i-1}^2 + y_j^2}} \right) - \frac{x_i}{2\Delta y} \left( \frac{a_{i,j+1}}{\sqrt{x_i^2 + y_{j+1}^2}} - \frac{a_{i,j-1}}{\sqrt{x_i^2 + y_{j-1}^2}} \right)}_{\text{advection } (u \cdot \nabla a)} + \underbrace{\frac{1}{\text{Pe}} \left( \frac{a_{i+1,j} - 2a_{i,j} + a_{i-1,j}}{\Delta x^2} + \frac{a_{i,j+1} - 2a_{i,j} + a_{i,j-1}}{\Delta y^2} \right)}_{\text{diffusion } (\kappa \Delta a)}}_{\text{reaction } (\text{Da}} \underbrace{\left( \frac{a_{i+1,j} - 2a_{i,j} + a_{i-1,j}}{\Delta x^2} + \frac{a_{i,j+1} - 2a_{i,j} + a_{i,j-1}}{\Delta y^2} \right)}_{\text{reaction } (\text{Da}} \underbrace{\left( \frac{a_{i+1,j} - 2a_{i,j} + a_{i-1,j}}{\Delta x^2} + \frac{a_{i,j+1} - 2a_{i,j} + a_{i,j-1}}{\Delta y^2} \right)}_{\text{reaction } (\text{Da}} \underbrace{\left( \frac{a_{i+1,j} - 2a_{i,j} + a_{i-1,j}}{\Delta x^2} + \frac{a_{i,j+1} - 2a_{i,j} + a_{i,j-1}}{\Delta y^2} \right)}_{\text{reaction } (\text{Da}} \underbrace{\left( \frac{a_{i+1,j} - 2a_{i,j} + a_{i-1,j}}{\Delta x^2} + \frac{a_{i,j+1} - 2a_{i,j} + a_{i,j-1}}{\Delta y^2} \right)}_{\text{reaction } (\text{Da}} \underbrace{\left( \frac{a_{i+1,j} - 2a_{i,j} + a_{i-1,j}}{\Delta x^2} + \frac{a_{i,j+1} - 2a_{i,j} + a_{i,j-1}}{\Delta y^2} \right)}_{\text{reaction } (\text{Da}} \underbrace{\left( \frac{a_{i+1,j} - 2a_{i,j} + a_{i-1,j}}{\Delta x^2} + \frac{a_{i,j+1} - 2a_{i,j} + a_{i,j-1}}{\Delta y^2} \right)}_{\text{reaction } (\text{Da}} \underbrace{\left( \frac{a_{i+1,j} - 2a_{i,j} + a_{i-1,j}}{\Delta x^2} + \frac{a_{i,j+1} - 2a_{i,j} + a_{i,j-1}}{\Delta y^2} \right)}_{\text{reaction } (\text{Da}} \underbrace{\left( \frac{a_{i+1,j} - 2a_{i,j} + a_{i,j-1}}{\Delta x^2} + \frac{a_{i,j+1} - 2a_{i,j} + a_{i,j-1}}{\Delta y^2} \right)}_{\text{reaction } (\text{Da}} \underbrace{\left( \frac{a_{i+1,j} - 2a_{i,j} + a_{i,j-1}}{\Delta x^2} + \frac{a_{i,j+1} - 2a_{i,j}}{\Delta x^2} \right)}_{\text{reaction } (\text{Da}} \underbrace{\left( \frac{a_{i+1,j} - 2a_{i,j} + a_{i,j-1}}{\Delta x^2} + \frac{a_{i+1,j} - 2a_{i,j}}{\Delta x^2} \right)}_{\text{reaction } (\text{Da}} \underbrace{\left( \frac{a_{i+1,j} - 2a_{i,j} + a_{i,j-1}}{\Delta x^2} + \frac{a_{i+1,j} - 2a_{i,j}}{\Delta x^2} \right)}_{\text{reaction } (\text{Da}} \underbrace{\left( \frac{a_{i+1,j} - 2a_{i,j} + a_{i,j-1}}{\Delta x^2} + \frac{a_{i+1,j} - 2a_{i,j}}{\Delta x^2} \right)}_{\text{reaction } (\text{Da}} \underbrace{\left( \frac{a_{i+1,j} - 2a_{i,j} + a_{i,j-1}}{\Delta x^2} + \frac{a_{i+1,j} - 2a_{i,j}}{\Delta x^2} \right)}_{\text{reaction } (\text{Da}} \underbrace{\left( \frac{a_{i+1,j} - 2a_{i,j} + a_{i,j-1}}{\Delta x^2} + \frac{a_{i+1,j} - 2a_{i,j}}{\Delta x^2} \right)}_{\text{reaction } (\text{Da}} \underbrace{\left( \frac{a_{i+1,j} - 2a_{i,j} + a_{i,j-1}}{\Delta x^2} + \frac{a_{i+1,j} - 2a$$

For a product coherent state at time t, write  $z_{i,j} := \langle a_{i,j} \rangle_t$ . Using the normal-order rule,

$$F_{i,j}(z) = \frac{y_j}{2\Delta x} \left( \frac{z_{i+1,j}}{\sqrt{x_{i+1}^2 + y_j^2}} - \frac{z_{i-1,j}}{\sqrt{x_{i-1}^2 + y_j^2}} \right) - \frac{x_i}{2\Delta y} \left( \frac{z_{i,j+1}}{\sqrt{x_i^2 + y_{j+1}^2}} - \frac{z_{i,j-1}}{\sqrt{x_i^2 + y_{j-1}^2}} \right) + \frac{1}{\text{Pe}} \left( \frac{z_{i+1,j} - 2z_{i,j} + z_{i-1,j}}{\Delta x^2} + \frac{z_{i,j+1} - 2z_{i,j} + z_{i,j-1}}{\Delta y^2} \right) + \text{Da} \left( z_{i,j} - z_{i,j}^2 \right).$$
(C58)

a. Forward-Euler mean update. From Sec. C3, the coherent-state matrix elements lead to the same algebraic cancellation as in 1D, yielding

$$z_{i,j}(t + \Delta t) = z_{i,j}(t) + \Delta t F_{i,j}(z(t)) + O(\Delta t^2), \qquad F_{i,j}(z) \text{ given by (C58)}.$$
 (C59)

b. First order variance Let  $\operatorname{Var}_{i,j}(t) := \operatorname{Var}(a_{i,j}) = \langle a_{i,j}^{\dagger} a_{i,j} \rangle_t - |\langle a_{i,j} \rangle_t|^2$ . Exactly the same dimension-independent algebra as in Sec. C 3 shows that

$$\operatorname{Var}_{i,j}(t+\Delta t) = \left(1 - 2\Delta t \operatorname{Re}\Sigma(z(t))\right) \operatorname{Var}_{i,j}(t) + O(\Delta t^2), \quad \text{hence if } \operatorname{Var}_{i,j}(t) = 0, \ \operatorname{Var}_{i,j}(t+\Delta t) = O(\Delta t^2), \quad \text{(C60)}$$
 where  $\Sigma(z) = \sum_{i,j} z_{i,j}^* F_{i,j}(z).$ 

c. Analysis of Numerical Stability. Write  $\Sigma(z) = \Sigma_{\rm adv}(z) + \Sigma_{\rm diff}(z) + \Sigma_{\rm reac}(z)$ . Introduce forward differences  $\delta_x^+ z_{i,j} := z_{i+1,j} - z_{i,j}$ ,  $\delta_y^+ z_{i,j} := z_{i,j+1} - z_{i,j}$ , and the discrete Laplacian  $\Delta_h z_{i,j} := \frac{\delta_x^+ z_{i,j} - \delta_x^+ z_{i-1,j}}{\Delta x^2} + \frac{\delta_y^+ z_{i,j} - \delta_y^+ z_{i,j-1}}{\Delta y^2}$ . Under periodic (or homogeneous) boundary conditions, discrete summation by parts in 2D gives

$$\sum_{i,j} z_{i,j}^* \Delta_h z_{i,j} = -\sum_{i,j} \left( \frac{|\delta_x^+ z_{i,j}|^2}{\Delta x^2} + \frac{|\delta_y^+ z_{i,j}|^2}{\Delta y^2} \right), \tag{C61}$$

hence the diffusion contribution is strictly dissipative:

$$\operatorname{Re} \Sigma_{\operatorname{diff}}(z) = \frac{1}{\operatorname{Pe}} \operatorname{Re} \sum_{i,j} z_{i,j}^* \Delta_h z_{i,j} = -\frac{1}{\operatorname{Pe}} \sum_{i,j} \left( \frac{|\delta_x^+ z_{i,j}|^2}{\Delta x^2} + \frac{|\delta_y^+ z_{i,j}|^2}{\Delta y^2} \right) \le 0.$$
 (C62)

For the advection part (real if z is globally real but not sign-definite in general), using Young's inequality with any  $\epsilon > 0$ , and denoting  $||z||_{\infty} := \max_{i,j} |z_{i,j}|, ||w||_1 := \sum_{i,j} |w_{i,j}|,$  one obtains

$$\left| \Sigma_{\text{adv}}(z) \right| \le C_u \left( \frac{\|\delta_x^+ z\|_1}{\Delta x} + \frac{\|\delta_y^+ z\|_1}{\Delta y} \right) \le \frac{\epsilon}{\text{Pe}} \sum_{i,j} \left( \frac{|\delta_x^+ z_{i,j}|^2}{\Delta x^2} + \frac{|\delta_y^+ z_{i,j}|^2}{\Delta y^2} \right) + \frac{C_u^2 \text{Pe}}{4\epsilon} N_{xy},$$
 (C63)

where  $C_u := \frac{1}{2} \max_{i,j} \left( \frac{|y_j|}{\sqrt{x_i^2 + y_j^2}} + \frac{|x_i|}{\sqrt{x_i^2 + y_j^2}} \right)$  bounds the discrete velocity prefactor and  $N_{xy}$  is the number of grid points. For

$$\Sigma_{\text{reac}}(z) = \text{Da} \sum_{i,j} \left( z_{i,j}^* z_{i,j} - z_{i,j}^* z_{i,j}^2 \right).$$
 (C64)

If  $z_{i,j} \in \mathbb{R}$  (global phase fixed), then  $\Sigma_{\mathrm{reac}}(z) = \mathrm{Da} \sum_{i,j} \left( z_{i,j}^2 - z_{i,j}^3 \right)$ , which is positive for small amplitudes  $(z \ll 1$ , linear growth) and becomes negative for large z (nonlinear saturation), reflecting the Fisher–KPP mechanism. For complex z, use  $\left| \sum z^* z^2 \right| \leq \sum |z|^3 \leq \frac{2}{3} \sum |z|^2 + \frac{1}{3} \sum |z|^4$  to bound  $\mathrm{Re} \ \Sigma_{\mathrm{reac}}$ .

d. Summary for the Fisher-KPP step. Given  $F_{i,j}(z)$  in (C58) and  $\Sigma(z)$  as above, one step of the 2D Fisher update obeys

$$z_{i,j}(t+\Delta t) = z_{i,j}(t) + \Delta t F_{i,j}(z(t)) + O(\Delta t^2), \quad \operatorname{Var}_{i,j}(t+\Delta t) = (1 - 2\Delta t \operatorname{Re} \Sigma(z(t))) \operatorname{Var}_{i,j}(t) + O(\Delta t^2), \quad (C65)$$

with Re  $\Sigma_{\text{diff}}(z) \leq 0$  strictly dissipative by (C62), advection controlled by (C63), and reaction providing growth at small amplitude and saturation at large amplitude. In diffusive/saturated regimes the normalized denominator  $1+2\Delta t \operatorname{Re}\Sigma(z)$  remains well-conditioned, ensuring stable first-order evolution.

#### Appendix D: Trotterization time-evolution algorithm for solving Lid-Driven Cavity Problem

Each discrete stream function and vorticity component at grid location (i, j) is embedded into the continuous-variable framework by associating two coherent-state amplitudes,  $z_{i,j}^{(\omega)}$  and  $z_{i,j}^{(\psi)}$ , corresponding to  $\omega_{i,j}$  and  $\psi_{i,j}$  respectively. Independent bosonic modes are assigned so that

$$|z\rangle = \bigotimes_{i,j} |z_{i,j}^{(\omega)}\rangle \otimes |z_{i,j}^{(\phi)}\rangle,$$
 (D1)

and the dynamical variables are recovered via Eq. (2). The discrete Navier-Stokes evolution is lifted into the bosonic operator generator by replacing each field with the corresponding annihilation operators. For instance, Eq. (D11b) is encoded schematically as:

$$F_{i,j}^{\psi}(a) = \frac{1}{\Delta x^2} \left( a_{i+1,j}^{\psi} - 2a_{i,j}^{\psi} + a_{i-1,j}^{\psi} \right) + \frac{1}{\Delta y^2} \left( a_{i,j+1}^{\psi} - 2a_{i,j}^{\psi} + a_{i,j-1}^{\psi} \right) + a_{i,j}^{\omega},$$

and will be time-evolved with the Hamiltonian-like operator  $M^{\psi} = \sum_{i,j} a_{i,j}^{\psi^{\dagger}} F_{i,j}^{\psi}(a)$ a. Mean Update: Trotterization Methods Unlike the derivation in 2D Fisher-KPP equation, we use a Trotterized (Suzuki-Trotter) update to compute the mean-field dynamics for lid-driven cavity problem as an alternative approach. The finite-time update follows Eq. (C6) and can be written as:

$$z_k(t + \Delta t) = \frac{\langle z(t)|e^{M^{\dagger}\Delta t} a_k e^{M\Delta t}|z(t)\rangle}{\langle z(t)|e^{M^{\dagger}\Delta t}e^{M\Delta t}|z(t)\rangle}.$$
 (D2)

To act on  $a_k$  it is convenient to move  $a_k$  through  $e^{M\Delta t}$  using the Baker–Campbell–Hausdorff (BCH)/Campbell lemma identity:

$$e^{-X}Ye^X = \sum_{n=0}^{\infty} \frac{[Y,X]_n}{n!},$$
 (D3)

where  $[Y, X]_n = [[\dots [[Y, X], X], \dots, X], X]$  is the *n*-times iterated commutator. Choosing  $X = M\Delta t$  and  $Y = a_k$  yields

$$a_k e^{M\Delta t} = e^{M\Delta t} (a_k + [a_k, M]\Delta t + \frac{1}{2}[[a_k, M], M]\Delta t^2 + \mathcal{O}(\Delta t^3)).$$
 (D4)

Substituting Eq. (D4) into the numerator and canceling the common factor  $e^{M^{\dagger}\Delta t}e^{M\Delta t}$  between the numerator and denominator gives, to second order

$$z_k(t + \Delta t) = \frac{\langle z(t)|a_k + [a_k, M]\Delta t + \frac{1}{2}[[a_k, M], M]\Delta t^2|z(t)\rangle}{\langle z(t)|z(t)\rangle} + \mathcal{O}(\Delta t^3). \tag{D5}$$

The first commutator reduces to

$$[a_k, M] = \sum_j [a_k, a_j^{\dagger}] F_j(a) = F_k(a),$$
 (D6)

which shows that the linear term in  $\Delta t$  produces  $F_k(a)$ . For the quadratic term, the identity

$$[[a_k, M], M] = [F_k(a), \sum_j a_j^{\dagger} F_j(a)] = \sum_j [F_k(a), a_j^{\dagger}] F_j(a), \tag{D7}$$

is needed. The commutator  $[F_k(a), a_j^{\dagger}]$  is evaluated next. Let  $F_k(a)$  be normally ordered and analytic, with power-series expansion  $F_k(a) = \sum_{\alpha} c_{\alpha} \prod_{\ell} a_{\ell}^{\alpha_{\ell}}$ . Then,

$$[F_k(a), a_j^{\dagger}] = \sum_{\alpha} c_{\alpha} \alpha_j a_j^{\alpha_j - 1} \prod_{\ell \neq j} a_{\ell}^{\alpha_{\ell}} = \frac{\partial F_k}{\partial a_j}(a).$$
 (D8)

This follows by linearity and  $[a_{\ell}, a_i^{\dagger}] = \delta_{\ell j}$ . Using Eq. (D8) in Eq. (D7) gives

$$[[a_k, M], M] = \sum_{i} \frac{\partial F_k}{\partial a_j}(a) F_j(a).$$
 (D9)

Inserting Eqs. (D6) and (D9) into Eq. (D5) and applying the coherent-state expectation value yields

$$z_k(t + \Delta t) = z_k(t) + F_k(z)\Delta t + \frac{1}{2} \sum_j \frac{\partial F_k}{\partial z_j}(z) F_j(z) \Delta t^2 + \mathcal{O}(\Delta t^3), \tag{D10}$$

which is precisely the second-order Taylor expansion of the classical flow map generated by  $\dot{z} = F(z)$ . Truncation in first order recovers Eq. (C16), i.e. the forward Euler update.

Now we consider the lid-driven cavity problem. The system is governed by the incompressible Navier-Stokes equations, written in stream-function-vorticity formulation:

$$\frac{\partial \omega}{\partial t} + \frac{\partial \psi}{\partial y} \frac{\partial \omega}{\partial x} - \frac{\partial \psi}{\partial x} \frac{\partial \omega}{\partial y} = \frac{1}{\text{Re}} \nabla^2 \omega, \tag{D11a}$$

$$\nabla^2 \psi = -\omega. \tag{D11b}$$

Here  $\psi$ ,  $\omega$ , and the velocity field  $\mathbf{u} = (u, v)$  are connected via

$$u = \frac{\partial \psi}{\partial y}, \quad v = -\frac{\partial \psi}{\partial x}, \quad \omega = \frac{\partial v}{\partial x} - \frac{\partial u}{\partial y},$$
 (D12)

and Re is the Reynolds number defined based on the velocity of the lid and the length of the cavity. The physical domain is the unit square  $\Omega = [0,1] \times [0,1]$ . The no-slip boundary conditions are imposed on the three stationary walls  $\mathbf{u}(x,0) = \mathbf{u}(0,y) = \mathbf{u}(1,y) = \mathbf{0}$ , while the top lid (y=1) is driven with a unit horizontal velocity  $\mathbf{u}(x,1) = (1,0)$ . The spatial domain is discretized using a uniform finite-difference grid with  $N_x \times N_y$  interior points. Standard second-order central differences are used to approximate spatial derivatives. In each time step,  $\omega$  is updated from Eq. (D11a) by advancing in time according to the Eq. (D10) update rule. Afterwards,  $\psi$  is updated from Eq. (D11b) by time-evolving the equation

$$\frac{\partial \psi}{\partial t} = \nabla^2 \psi + \omega,\tag{D13}$$

to reach the steady state.

Our numerical simulation shows that our methods can capture complex behavior under different Reynolds numbers. The steady state solution of the lid-driven cavity is shown in Fig. 5. The initial condition is zero for all grid points. The simulations were performed in two setups: one with  $N_x = N_y = 128$  grid and Re = 1,000, and another with  $N_x = N_y = 256$  grid and Re = 10,000. The vorticity field  $\omega$  advances in time with a time step of  $\Delta t = 0.005$ . The streamfunction  $\psi$  advances with the time step  $\Delta \tau = 5 \times 10^{-6}$  until convergence. The simulations continue until  $\|\omega(t + \Delta t) - \omega(t)\|_F \le 10^{-5}$ , where  $\|.\|_F$  is the Frobenius norm. The solution field obtained is in agreement with the direct numerical simulation (DNS) in previous works [76, 77], establishing the validity of the results.

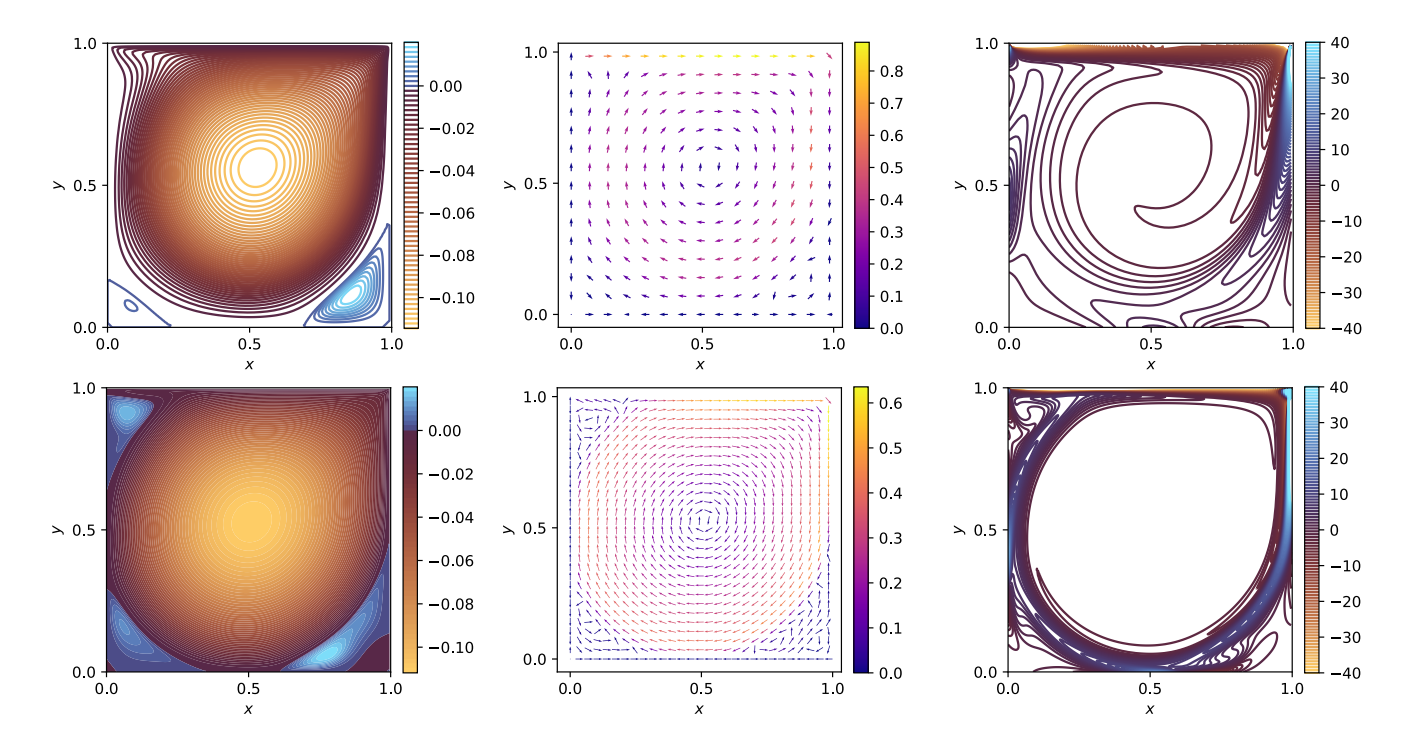


FIG. 5. The lid-driven cavity simulation with a  $128 \times 128$  grid and Re = 1000 in top row and a  $256 \times 256$  grid and Re = 10000 in bottom row. All panels show the flow at the steady state. *Left:* Contour plots of the stream function  $\psi$ . *Middle:* The velocity field  $\mathbf{u} = (u, v)$ . *Right:* The vorticity  $\omega$ . Simulation is done using bosonic simulator. The evolution follows the Euler update rule, and therefore, matches with DNS calculation.

#### Appendix E: Tensor Network Simulation of the Burgers' Equation

In order to assess the feasibility of the Trotterized time-evolution scheme used in this work, we simulate the viscous Burgers' equation on a one-dimensional lattice with L=128 sites and Dirichlet boundary conditions at the two ends of the domain. The velocity field u(x,t) is discretized as  $u_j(t) \equiv u(x_j,t)$  at lattice points  $x_j$ , and its dynamics is approximated by Hamiltonian-like operator representing the finite-difference scheme. We employ the TEBD algorithm with a Trotterized time-evolution operator and a fixed time step of  $\Delta t=10^{-5}$ . Each lattice site is represented by a local bosonic Hilbert space, truncated to a maximum photon occupation number of  $n_{\rm max}=5$ . This cutoff corresponds to a local dimension of  $d=n_{\rm max}+1$  and was found to be the smallest value that yields numerically stable and visually accurate dynamics for the parameter regime considered. Figure 6 shows the simulated profiles at times t=0,0.06,0.12, and 0.18. Starting from a smooth Gaussian initial condition, the tensor network time evolution correctly captures both the steepening of the profile and the subsequent viscous smoothing, reproducing the shock-like structure and its broadening in time. Within plotting resolution, the TN results are indistinguishable by eye from the reference solution shown in Fig. 3, indicating that the Trotterized scheme is capable of faithfully reproducing Burgers' dynamics with a modest local truncation and time step.

#### Appendix F: Open-System Dynamics in the P-Representation: Detailed Derivation

This section expands the derivation of the PDE that governs the Glauber–Sudarshan P-function and the resulting evolution of the coherent-state amplitudes in the presence of photon loss. The density operator is expanded as

$$\rho(t) = \int d^2z \, P(z, z^*, t) \, |z\rangle\langle z|, \qquad d^2z \equiv \prod_j d^2z_j. \tag{F1}$$

The evolution of density matrix under the generator  $M = \sum_j a_j^{\dagger} F_j(a)$  and photon loss at the rate  $\gamma$  are governed by Eq. (10), which takes the form

$$\frac{\partial \rho}{\partial t} = \sum_{j} \left[ a_{j}^{\dagger} F_{j}(a) \rho + \rho F_{j}^{\dagger}(a) a_{j} + \gamma a_{j} \rho a_{j}^{\dagger} - \frac{\gamma}{2} a_{j}^{\dagger} a_{j} \rho - \frac{\gamma}{2} \rho a_{j}^{\dagger} a_{j} \right]. \tag{F2}$$

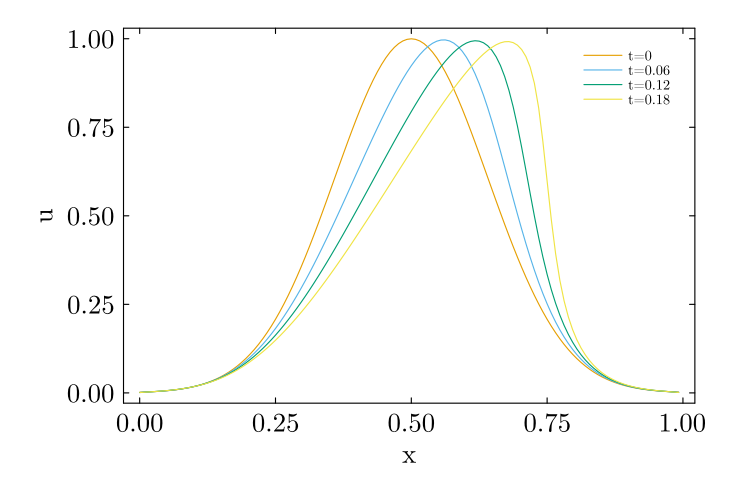


FIG. 6. Tensor network simulation of the Burgers' equation using a Trotterized TEBD time-evolution scheme. The initial condition is a Gaussian velocity profile, which evolves into a shock-like structure that is subsequently smoothed by viscosity. The resulting profiles at t = 0, 0.06, 0.12, and 0.18 are in excellent visual agreement with the reference solution shown in Fig. 3.

For the effect of  $a_j^{\dagger}$  and  $a_j$  on the density matrix basis  $|z\rangle\langle z|$ , integration by parts for  $a_j^{\dagger}|z\rangle\langle z|$  and  $|z\rangle\langle z|a_j$  yields the convenient differential actions

$$a_{j}^{\dagger} |z\rangle \langle z| = \left(-\partial_{z_{j}} + z_{j}^{*}\right) |z\rangle \langle z|,$$
 (F3)

$$|z\rangle\langle z| \ a_j = \left(-\partial_{z_j^*} + z_j\right)|z\rangle\langle z|.$$
 (F4)

when the derivatives are understood to act on everything to their right inside the P-integral. From moving  $\partial/\partial z_j$  and  $\partial/\partial z_j^*$  off the kets/bras onto P by parts, boundary terms vanish under the standard assumption that P decays sufficiently rapidly at  $|z| \to \infty$ . Using Eqs. (F3)–(F4) and normal ordering of  $F_j(a)$ , the coherent and dissipative components in Eq. (F2) are obtained as

$$M\rho = \int d^2z P(z, z^*, t) \sum_j F_j(z) a_j^{\dagger} |z\rangle \langle z| = \int d^2z \sum_j \left( -\frac{\partial}{\partial z_j} + z_j^* \right) \left[ P(z, z^*, t) F_j(z) \right] |z\rangle \langle z|, \tag{F5}$$

$$\rho M^{\dagger} = \int d^2z \, P(z, z^*, t) \sum_j F_j(z^*) \, |z\rangle \langle z| a_j = \int d^2z \sum_j \left( -\frac{\partial}{\partial z_j^*} + z_j \right) \left[ P(z, z^*, t) \, F_j(z^*) \right] |z\rangle \langle z|, \tag{F6}$$

$$\sum_{j} \gamma a_{j} \rho a_{j}^{\dagger} = \gamma \int d^{2}z \, P(z, z^{*}, t) \sum_{j} |z_{j}|^{2} |z\rangle\langle z|, \tag{F7}$$

$$-\frac{\gamma}{2}\sum_{j}\left(a_{j}^{\dagger}a_{j}\rho+\rho a_{j}^{\dagger}a_{j}\right)=-\frac{\gamma}{2}\int d^{2}z\sum_{j}\left[\left(-\frac{\partial}{\partial z_{j}}+z_{j}^{*}\right)\!\left(Pz_{j}\right)+\left(-\frac{\partial}{\partial z_{j}^{*}}+z_{j}\right)\!\left(Pz_{j}^{*}\right)\right]|z\rangle\langle z|.\tag{F8}$$

Here and below,  $P \equiv P(z, z^*, t)$  is used for compactness. Collecting Eqs. (F5)–(F8) in Eq. (F2) and comparing the coefficients of  $|z\rangle\langle z|$  gives the first-order PDE

$$\frac{\partial P}{\partial t} = \sum_{j} \left[ \frac{\partial}{\partial z_{j}} \left( \frac{\gamma}{2} z_{j} P - F_{j}(z) P \right) + \frac{\partial}{\partial z_{j}^{*}} \left( \frac{\gamma}{2} z_{j}^{*} P - F_{j}(z^{*}) P \right) + \left( z_{j}^{*} F_{j}(z) + z_{j} F_{j}(z^{*}) \right) P \right]. \tag{F9}$$

The last term arises from the  $z_j^*$  and  $z_j$  components in Eqs. (F3)–(F4). This term reflects the change in the norms of coherent states. In practice, calculations are performed at each time step. Therefore, the norm can be restored to the coherent states so that the normalization of  $\rho$  is preserved by Eq. (F9). The PDE can be viewed as a generalized drift equation for P, with photon

loss adding a linear contraction in phase space. Let  $\langle\!\langle g \rangle\!\rangle \equiv \int d^2z \, g(z,z^*) \, P(z,z^*,t)$  denote P-averages. For the first moments  $z_k$ 

$$\frac{d}{dt}\langle\langle z_k\rangle\rangle = \int d^2z \, z_k \, \frac{\partial P}{\partial t}.\tag{F10}$$

Note that the first moment can also be seen as the expectation values of the annihilation operator, namely

$$\langle a_k \rangle = \operatorname{Tr}(a_k \rho) = \int d^2 z \, P(z, z^*, t) z_k \operatorname{Tr}(|z\rangle \langle z|) = \int d^2 z \, P(z, z^*, t) z_k = \langle \langle z_k \rangle \rangle. \tag{F11}$$

Insertion of Eq. (F9) and integration by parts (with vanishing boundary terms) give

$$\frac{d}{dt}\langle\langle z_k\rangle\rangle = -\left\langle\langle\frac{\gamma}{2}z_k - F_k(z)\right\rangle\rangle + \sum_j \left\langle\langle z_r z_j^* F_j(z) + z_r z_j F_j(z^*)\right\rangle\rangle. \tag{F12}$$

For sharply peaked P (Gaussian-like packet centered at z with small covariance), the factorization

$$\langle\langle G(a, a^{\dagger})\rangle\rangle \approx G(\langle\langle z\rangle\rangle, \langle\langle z^*\rangle\rangle),$$
 (F13)

holds for normally ordered G, where G denotes any normally ordered polynomial or analytic function of the mode operators (e.g. finite sums of monomials). In the Glauber–Sudarshan P-representation one has the exact mapping  $\langle G(a,a^{\dagger})\rangle = \int d^2z \, P(z,z^*,t)G(z,z^*)$  [78–82]. If P is Gaussian-like and narrow with covariance  $\Sigma$ , a Taylor expansion about the mean z shows the leading correction is  $O(\|\Sigma\|)$ , so evaluating G at the means gives the standard mean-field (Gaussian) closure [79–85]. Under this closure, Eq. (F12) reduces to

$$\frac{dz_k}{dt} = F_k(z) - \frac{\gamma}{2} z_k,\tag{F14}$$

where  $z_k \equiv \langle \langle z_k \rangle \rangle = \langle a_k \rangle$ . Equation (F14) reproduces the drift stated in the main text, implying an exponential decay of the coherent amplitude by  $\exp(-\gamma t/2)$ .